Engineering Fracture Mechanics xxx (xxxx) xxx–xxx

Contents lists available at ScienceDirect

Engineering Fracture Mechanics

journal homepage: www.elsevier.com/locate/engfracmech

Unstable crack growth in hydraulic fracturing: The combined effects of pressure and shear stress for a power-law fluid

Wenhao Shen[a,b], Fuqian Yang[c], Ya-Pu Zhao[a,b,*]

[a] State Key Laboratory of Nonlinear Mechanics (LNM), Institute of Mechanics, Chinese Academy of Sciences, Beijing 100190, China
[b] School of Engineering Science, University of Chinese Academy of Sciences, Beijing 100049, China
[c] Department of Chemical and Materials Engineering, University of Kentucky, Lexington, KY 40506, USA

ARTICLE INFO

Keywords:
Hydraulic fracturing
Full-stress model
Shear stress
Unstable crack
Crack-closure criterion

ABSTRACT

The underlying mechanisms of hydraulic fracturing remain elusive, and the optimization of the related processes for rocks of low permeability is challenging. There exists local crack closure induced by shear stress, which is one of the crack instabilities for a straight crack. In this study, we develop a full-stress model, which includes the combined effects of hydrodynamic pressure and shear stress on the crack surfaces. The hydrodynamic pressure is a driving force, while the shear stress is a resistance force. A novel criterion for crack propagation is derived based on the asymptotic solution of shear stress. The asymptotic solution, which is derived using perturbation analysis in the toughness-dominant regime, reveals the existence of the crack-closure phenomenon and shear-stress-dominant regime. The necessary condition for the crack closure is obtained according to numerical calculations. An energy analysis is conducted to discuss the difference between the shear-stress-dominant and the viscosity-dominant regimes. The existence of the crack closure is shown to be independent of two assumptions, lubrication theory and no-fluid-lag zone. The results presented in this study are useful for the simulation and design of hydraulic fracturing.

Nomenclature

C, n	flow consistence index, flow behavior index, $C' = C \times 2^{2n+1}[(2n+1)/2n]^n$
$\widetilde{C}$, $\widetilde{K}_{IC}$, $\widetilde{Q}$, $\widetilde{\gamma}$	dimensionless quantities in the time-independent system of units
E, ν	Young's modulus, Poisson's ratio, $E' = E/(1-\nu^2)$
e_p, e_t	power indexes of pressure and shear stress
G, G_C	energy release rate, critical energy release rate
K_I, K_{IC}	mode-I stress intensity factor, fracture toughness
$\mathscr{K}$, $\mathscr{Q}$, $\mathscr{R}$	dimensionless quantities in the time-dependent system of units
l, l_f, l_0	half crack length, half length of the fluid region, initial half crack length
$\mathscr{M}$, $\mathscr{P}$, $\mathscr{S}$, $\mathscr{V}$	dimensionless quantities used to build the time-dependent system of units
p, p_v	net pressure in the fracturing fluid, vapor pressure in the fluid-lag zone
q, q_0	flow rate, flow rate at the wellbore
w	crack opening

* Corresponding author at: State Key Laboratory of Nonlinear Mechanics (LNM), Institute of Mechanics, Chinese Academy of Sciences, Beijing 100190, China.
E-mail address: yzhao@imech.ac.cn (Y.-P. Zhao).

https://doi.org/10.1016/j.engfracmech.2018.11.032
Received 10 May 2018; Received in revised form 9 September 2018; Accepted 16 November 2018

$\Delta\widetilde{x}_{cr}$	critical mesh size
γ, θ	surface tension and contact angle of fracturing fluid
ε, P, T	time-independent quantities
η	power (energy rate), subscripts "tot", "frac", "visc" and "strain" represent the total added energy rate, the power used for fracturing, the viscous dissipation rate and the change rate of the strain energy, respectively
μ	dynamic viscosity of fracturing fluid
σ_∞	crustal stress
τ	shear stress acting on the crack surfaces

Subscripts "p" and "t" represent the pressure and the shear stress, respectively.
The symbol "~" above a variable represents that the variable is dimensionless.

1. Introduction

Analyzing hydraulic fracturing has been a topic of great interest since 1947. The difficulties of analyzing this process lie in the strong coupling between elastic deformation and viscous flow, moving crack and fluid tips. Mathematical models [1–9], which differ either in geometry or physical effect, have been proposed to predict the dimensions of fracture and the wellbore pressure.

There are reports that suggest the presence of a boundary layer near the crack tip with an abnormal stress singularity in its outer solution [3,10]. This result is due to the competition between the fracture of the solid and the viscous dissipation of the fracturing fluid. The size of the boundary layer is determined by a single dimensionless parameter (called the dimensionless fracture toughness), which represents the ratio of fracturing energy to the energy of viscous dissipation [10]. A viscosity-dominant regime (or a toughness-dominant regime) is achieved when this parameter approaches zero (or infinity). A small boundary layer corresponds to a small value of this dimensionless parameter. The factors that influence the stress singularity of the outer solution include the compressibility, laminar or turbulent flow state and leakage of the fracturing fluid [4,11]. It is worth pointing out that only the coupling between the pressure and the normal stress on the solid-liquid interface is considered in the derivation of outer solution [3,10], and the effect of the flow-induced shear stress is neglected.

Recently, flow-induced shear stress has been found to play a more important role than hydrodynamic pressure in the outer solution, since the singularity of shear stress is much stronger than that of the hydrodynamic pressure [6,7]. Different from hydrodynamic pressure, flow-induced shear stress tends to inhibit the crack propagation. The strong singularity of the flow-induced shear stress leads to the breakdown of the criteria commonly used for the crack propagation and deflection in the viscosity-dominant regime [6,7], even though the flow-induced shear stress is negligible in the calculation of the crack opening far away from the crack tip [8]. There likely exists potential unstable crack growth caused by the flow-induced shear stress, and the criteria for crack propagation needs to be modified in the toughness-dominant regime [6,7]. Unstable crack growth is important because it may lead to the formation of a crack network, which is of practical importance in many fields, including reservoir stimulation in shale gas exploitation [12]. Shen and Zhao [6,7] discussed the hydraulic-crack growth in a homogeneous medium, and showed potential deflections of fluid-driven cracks. Their results provide some novel insights into the control of the crack path.

In their analyses [6,7], Shen and Zhao showed the crack-closure phenomenon on the basis of the local asymptotic solution at the crack tip and the one-way coupling between the fracture of rocks and the viscous flow of fracturing fluid. The potential of local crack closure near the crack tip is a sign of instabilities if a crack is assumed to propagate straightly. Different from a dynamic crack, of which the unstable growth is predicted with the near-crack-tip maximum tensile stress or strain energy density [13,14], the shear-stress-induced crack-closure phenomenon was demonstrated by a negative crack opening [6,7]. Also, there are a variety of factors that affect the crack-closure phenomenon: lubrication theory (in which the vertical velocity is neglected) [15] and fluid-lag zone [2,10]. These factors remove the stress singularity which is the basis of the asymptotic analysis of Refs. [6,7]. Consequently, global solutions, which are the solutions to the fully coupled solid-fluid problem and are applicable to the whole crack surfaces, are needed to study the unstable crack growth, and the effects of lubrication theory and fluid-lag zone are needed to be evaluated.

Although the near-crack-tip asymptotics reveals possible occurrence of local crack closure in the viscosity-dominant regime [6,7], there are no reports available on the related results in the laboratory experiments [16–19]. There are several possibilities for the lack of reports on the crack-closure phenomenon, including (1) there is a criterion for the crack-closure phenomenon, (2) the crack is not straight, (3) the lubrication theory is invalid near the crack tip used in the asymptotic analysis [15], and (4) there is a fluid-lag zone which eliminates the singularities of pressure and shear stress [2,6]. Such behavior raises the question: is there an unstable crack growth with the presence of a fluid-lag zone or with a two-dimensional flow assumption near the crack tip? If so, what is the criterion for the unstable growth of a crack?

In this work, the shear-stress-induced unstable crack growth is studied by solving the global solution of the fully-coupled solid-fluid problem. As shown in Fig. 1, the highly pressurized fluid, which is forced into the crack, introduces stresses on the crack surfaces, resulting in the opening and propagation of the crack and creating a narrow channel in rock. Lubrication theory [20,21] is used to describe the viscous flow. The rock is considered as an infinite, impermeable, elastic space with a Griffith-type crack. The crack grows symmetrically about the wellbore, and the crack path is assumed straight. There is a fluid-lag zone between the tip of the fracturing fluid and the tip of the crack.

This paper is organized as follows. First, a full-stress model is developed by incorporating the flow-induced shear stress and hydrodynamic pressure. The surface tension of the fracturing fluid is introduced with the Young-Laplace equation [21]. A new criterion of the crack propagation is derived in the toughness-dominant regime. This full-stress model can be extended to model a real hydraulic fracturing. Second, for a fluid-driven crack with no fluid-lag zone, the crack-closure phenomenon is presented with perturbation analysis. By imposing two numerical constraints, mesh-dependent results due to the crack-closure phenomenon are shown,

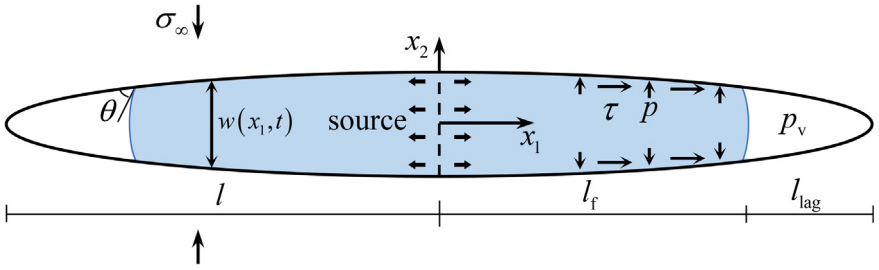

Fig. 1. Schematic of hydraulic fracturing, showing the flow of a viscous fluid into a Griffith-type crack at a constant flow rate.

and a semi-empirical criterion is obtained for the mesh-dependent results. The effect of lubrication theory on stress singularities is studied. Third, the effects of fluid-lag zone on the crack-closure phenomenon are studied, and the mechanism of the shear-stress-induced crack-closure is further discussed.

2. Problem formulation

A Cartesian coordinate system shown in Fig. 1 is used in the analysis with O being the inlet of the fracturing fluid, Ox_1 being parallel to the crack surfaces, and Ox_2 being perpendicular to the crack surfaces. For a Griffith-type crack in an infinite space, the crack opening, w, flow rate, q, hydrodynamic pressure, p, and shear stress, τ, are symmetric about both Ox_1 and Ox_2 axes. For simplification, both the governing and boundary-condition equations are described in the first quadrant, where $w \geqslant 0$.

The theories of lubrication flow and LEFM are used to analyze the hydraulic fracturing with the stress state being plane strain. The crack will propagate when the stress intensity factor is larger than the fracture toughness, K_{IC}, of the rock. The flow of the fracturing fluid into the channel between fracture surfaces leads to the opening of the fracture in the rock. In the full-stress model, both hydrodynamic pressure and shear stress are incorporated in the boundary conditions on the fluid-solid interface.

2.1. Viscous fluid flow in a narrow channel

The lubrication theory without the presence of inertial and body forces is used to describe the flow of the fracturing fluid [20,21]. It is known that the maximum pressure in hydraulic fracturing is $10^1 \sim 10^2$ MPa [22]. Thus, it is reasonable to assume the fracturing fluid as incompressible inside the crack. Note that the stress singularity associated with the viscous flow of fracturing fluid at the crack tip can be changed by considering the compressibility and phase transition. Here, we adopt the commonly used assumption of incompressible fluid for simplicity [1–3,11,23]. The flow behavior of the fracturing fluid follows the Ostwald-de Waele relationship, $\tau = C\dot{\gamma}^n$, where $\dot{\gamma}$ is shear rate, C and n are constants representing flow consistency index and flow behavior index, respectively. The Ostwald-de Waele model is applicable to both shear thinning and shear thickening fluids in addition to Newtonian fluids.

Using the condition of mass conservation, the differential equation describing the crack opening can be expressed as

$$\frac{\partial w(x_1, t)}{\partial t} + \frac{\partial q(x_1, t)}{\partial x_1} = 0 \tag{1}$$

in which $q(x_1, t)$ is the flow rate at location x_1 of the channel between the crack surfaces. According to the lubrication theory [20,21], the pressure gradient can be calculated from the flow rate as

$$\frac{\partial p(x_1, t)}{\partial x_1} = -\mathrm{sgn}\{q(x_1, t)\}\frac{C' |q(x_1, t)|^n}{[w(x_1, t)]^{2n+1}} \tag{2}$$

where sgn{*} is the signum function, and $C' = C \times 2^{2n+1}[(2n + 1)/2n]^n$. It is evident that a narrower fracture leads to a higher pressure gradient for the same flow rate. Note that hydraulic approximation was used in the derivation of Eq. (2), i.e., the velocity component perpendicular to the x_1 axis is negligible [24]. This approximation results in no vortex near the crack tip and an underestimated pressure drop. The flow rate is therefore a monotonous function of x_1, and the pressure gradient and shear stress do not change their signs. The force balance in the x_1 direction yields

$$\tau(x_1, t) = \frac{w(x_1, t)}{2}\frac{\partial p(x_1, t)}{\partial x_1} \tag{3}$$

The conditions of constant flow rate at the origin and the relationship between the fluid-tip position and the flow rate give the kinematic boundary conditions as

$$q(0, t) = q_0 \tag{4}$$

$$q(l_f(t), t) = \dot{l}_f(t) w(l_f(t), t) \tag{5}$$

where $l_f(t)$ is the position of the fluid tip and q_0 is the constant flow rate from wellbore. An alternative to Eq. (4) or (5) is the global mass balance as

$$q_0 t = \int_0^{l_f(t)} w(\zeta, t)\mathrm{d}\zeta \tag{6}$$

We assume that the fluid-lag zone is filled up with a vapor. The fluid pressure, the vapor pressure in the fluid-lag zone and the surface tension are balanced at the fluid tip. Using the Young-Laplace equation, one has

$$p(l_f(t), t) = p_v - \frac{\gamma \cos\theta}{w(l_f(t), t)} \tag{7}$$

where p_v is the pressure of the vapor, γ and θ are the surface tension and contact angle, respectively. Note that there are various models describing the motion of contact line either in the micro- or macroscale instead of the Young-Laplace equation [5,21].

2.2. Deformation of rocks

The fractured rock is assumed to be linear-elastic and brittle. There is only a Griffith-type crack in the fractured rock. The crack opening can be found as [6]

$$\begin{aligned} w(x_1, t) = {} & \frac{8}{\pi E'} \int_0^{l_f(t)} [p(\zeta, t) - p_v] \ln \frac{\sqrt{l^2(t) - x_1^2} + \sqrt{l^2(t) - \zeta^2}}{\sqrt{|x_1^2 - \zeta^2|}} \mathrm{d}\zeta \\ & + \frac{4(1-2\nu)}{(1-\nu)E'} \int_{x_1}^{l_f(t)} \tau(\zeta, t)\mathrm{d}\zeta + \frac{4(\sigma_\infty + p_v)}{E'} \sqrt{l^2(t) - x_1^2} \end{aligned} \tag{8}$$

where $E' = E/(1-\nu^2)$ with E being Young's modulus, ν being Poisson's ratio, σ_∞ the least compressive-principle stress in the rock, and $l(t)$ being the crack length.

Assume that the fluid-tip position at $t = t_0$ is l_{f0}, i.e.,

$$l_f(t_0) = l_{f0} \tag{9}$$

where t_0 is determined by the mass conservation. If there is no fluid-lag zone, $l_f(t) = l(t)$, without presence of the vapor pressure, Eqs. (4) and (7) are redundant. Eq. (5) degenerates to

$$q(l(t), t) = 0 \tag{10}$$

due to the finite crack-tip velocity and zero crack opening at the crack tip. The initial condition becomes $l(t_0) = l_0$. $p(x_1, t) - \sigma_\infty$, denoted as $p(x_1, t)$ for convenience, is used to eliminate the crustal stress.

2.3. Criterion for crack propagation

According to the result given by Shen and Zhao [6], the stress component, σ_{11}, is used to evaluate the stress intensity factor. There is

$$\begin{aligned} K_I = {} & 2\sqrt{\frac{l(t)}{\pi}} \int_0^{l_f(t)} \frac{p(\zeta, t)\mathrm{d}\zeta}{\sqrt{l^2(t) - \zeta^2}} + 4\sqrt{\frac{2}{\pi}} \lim_{x_1 \to l^+} \sqrt{x_1 - l(t)} \int_0^{l_f(t)} \frac{\tau(\zeta, t)\zeta \mathrm{d}\zeta}{x_1^2 - \zeta^2} \\ & + \sigma_\infty \sqrt{\pi l(t)} + p_v \left[\sqrt{\pi l(t)} - 2\sqrt{\frac{l(t)}{\pi}} \arcsin \frac{l_f(t)}{l(t)} \right] \end{aligned} \tag{11}$$

where K_I is the modified mode-I stress intensity factor. The crack propagates when

$$K_I \geqslant K_{IC} \tag{12}$$

in which K_{IC} is the mode-I fracture toughness. The second term on the right-hand side of Eq. (11) may take effect for $l_f(t) = l(t)$, i.e. there is no fluid-lag zone, which leads to $\tau = O[(1 - x_1^2/l^2)^{e_t}]$. This term becomes non-removable for $e_t = -1/2$ and becomes dominant for $e_t < -1/2$, which occur in the toughness-dominant regime and viscosity-dominant regime for Newtonian fracturing fluid, respectively [6,7]. In the viscosity-dominant regime, τ is $O[(l - x_1)^{-2/3}]$ and negative, and K_I is negative infinity. The crack cannot propagate according to the concept associated with the stress-intensity factor [6,7]. Consequently, there is, in the toughness-dominant regime,

$$K_I = 2\sqrt{\frac{l(t)}{\pi}} \int_0^{l(t)} \frac{p(\zeta, t)\mathrm{d}\zeta}{\sqrt{l^2(t) - \zeta^2}} + 2\tau_0 \sqrt{\pi l(t)} + (\sigma_\infty + p_v)\sqrt{\pi l(t)} \geqslant K_{IC} \tag{13}$$

where $\tau = \tau_0/\sqrt{1 - x_1^2/l^2} + O(\sqrt{1 - x_1^2/l^2})$, $\tau_0 < 0$. The detailed derivation of Eq. (13) is given in Appendix A. With the term of $2\tau_0\sqrt{\pi l(t)}$, the stress intensity factor is dependent on the local property of shear stress, because shear stress introduces the same order of the singularity to stress as induced by pressure. The effect of shear stress is dependent on its local property, while that of pressure is dependent on its distribution.

Note that Eq. (13) is incompatible with the energy release rate. Let K_{Ip} and K_{It} denote the stress intensity factor induced by the pressure and the shear stress, respectively. The energy release rate of a crack tip is

$$G = K_{Ip} \left[\frac{K_{Ip}}{E'} + \frac{(1-2\nu)\tau_0 \sqrt{\pi l}}{2(1-\nu)E'} \right] \tag{14}$$

The detailed derivation of Eq. (14) is given in Appendix A. The commonly used relation, $G = K_I^2/E'$, becomes invalid due to the singular shear stress. For cases with zero or weaker-singular shear stress, Eq. (14) degenerates to $G = K_I^2/E'$.

Let K_{IC} be the fracture toughness for pressure-only cases. Using the energy concept, $G \geqslant G_C = K_{IC}^2/E'$, the modified criterion for the crack propagation in terms of the stress intensity factor is

$$K_{Ip}\left[K_{Ip} + \frac{(1-2\nu)\tau_0\sqrt{\pi l}}{2(1-\nu)}\right] \geqslant K_{IC}^2 \tag{15}$$

The discrepancy between Eqs. (13) and (15) stems from the interaction between the pressure and the crack opening induced by the singular shear stress. For $\tau_0 < 0$, a conservative criterion is obtained from the energy release rate as

$$K_I = 2\sqrt{\frac{l(t)}{\pi}}\int_0^{l(t)} \frac{p(\zeta,t)\mathrm{d}\zeta}{\sqrt{l^2(t)-\zeta^2}} + \frac{(1-2\nu)\tau_0}{2(1-\nu)}\sqrt{\pi l(t)} + (\sigma_\infty + p_v)\sqrt{\pi l(t)} \geqslant K_{IC} \tag{16}$$

It is clear that Eq. (16) is valid for $\tau = O[(l-x_1)^{-1/2}]$. The additional term in Eq. (16) is slightly smaller (absolute value) than that in Eq. (13), because $(1-2\nu)/2(1-\nu) < 1$ for $0 < \nu < 0.5$.

2.4. Energy partition without fluid-lag zone

Energy analysis has been used [10,11] to discuss the role of viscous flow and fracturing in hydraulic fracturing. The total power during fracturing consists of the contributions of viscous dissipation rate, the energy release rate due to the crack propagation and the change rate of the strain energy. In general, it is a challenge to calculate the viscous dissipation rate. The major issue is that the integral of $\iint_{S^f} \sigma_{ij}^f \dot{\gamma}_{ji}\mathrm{d}S$ is divergent, in which the superscript "f" represents fluid. For a Newtonian fracturing fluid, the first-order asymptotic solutions of both the shear stress and the strain rate are $O(1-\tilde{x}_1)^{-1/2}$, leading to a logarithmic singularity at the crack tip and divergence of the integral. This result suggests that the viscous dissipation rate cannot be calculated directly from the integration of the energy dissipation rate for viscous flow.

Here, a concise method is used to calculate the viscous dissipation rate. The total energy rate added during the fracturing is calculated as

$$\eta_{tot}(t) = 2p(0,t)q_0 \tag{17}$$

for the flow of the fracturing fluid into the fracture at a constant flow rate. Note that both the body force and the inertia term are assumed to be negligible in the full-stress model. The viscous dissipation rate due to the flow of the fracturing fluid is equal to the difference between the total energy and the work done by the stresses acting on the crack surfaces, i.e., $\oint_\Gamma \boldsymbol{v}\cdot\boldsymbol{\sigma}\cdot\boldsymbol{n}\,\mathrm{d}\Gamma$ for a slit crack. Here $\boldsymbol{v}$ is the velocity of the crack surface, and $\boldsymbol{n}$ is the unit outward normal vector of the crack surface. Thus, the viscous dissipation rate is

$$\eta_{visc}(t) = 2p(0,t)q_0 - 2\int_0^{l(t)} p(x_1,t)\frac{\partial w(x_1,t)}{\partial t}\mathrm{d}x_1 \tag{18}$$

Note that Eq. (18) does not include the work done by the shear stress in the crack surfaces, because it is negligible compared with the work done by pressure ($\bar{\tau}\bar{u}_1/\bar{p}\bar{u}_2 \approx \bar{\tau}/\bar{p} \approx \bar{w}/\bar{l} << 0$, where the over-bar represents the average value). The energy dissipation rate due to local fracturing of the rock can be calculated from the energy release rate. Using the relationship of $G_C = K_{IC}^2/E'$, one obtains

$$\eta_{frac}(t) = 2G_C\dot{l}(t) = 2\frac{K_{IC}^2}{E'}\dot{l}(t) \tag{19}$$

The change rate of the strain energy in the rock is calculated as

$$\eta_{strain}(t) = \eta_{tot}(t) - \eta_{visc}(t) - \eta_{frac}(t) \tag{20}$$

3. Hydraulic fracture with no fluid-lag zone

For hydraulic fractures without fluid-lag zone, there is crack closure in the fluid-tip region or deflection for the mode-I hydraulic fracture in the viscosity-dominant regime [6]. Shen and Zhao [6] used one-way coupling and asymptotic analysis to study the effect of shear stress on the crack opening and stress intensity factor via the solution of the pressure-only problem. Here, perturbation analysis and numerical calculation are used to obtain the global solution (the solution for arbitrary point in the domain of definition) with strong coupling between the lubrication theory and LEFM.

3.1. In toughness-dominant regime

3.1.1. Normalization

In the hydraulic fracturing field, both the time and length scales range largely. But a time-dependent unit system [23] was not used here, because the non-zero dimensionless parameters leads to additional derivatives with respect to time in the mass conservation equation. The normalization scheme is as follows

$$x_1 = l_0\widetilde{l}(\widetilde{t})\widetilde{x}_1,\ w(x_1,t) = \varepsilon l_0\widetilde{w}(\widetilde{x}_1,\widetilde{t}),\ p(x_1,t) = P\widetilde{p}(\widetilde{x}_1,\widetilde{t}) \text{ and } t = T\widetilde{t} \tag{21}$$

in which ε, P and T are time-independent quantities, which can be obtained by substituting Eq. (21) into Eqs. (1)–(3), (6), (8) and (16). The mass conservation must be preserved, and the pressure-induced crack opening is used to measure the overall crack opening. Consequently, Eq. (6) and the first term of the right-hand side of Eq. (8) are normalized. In the toughness-dominant regime, the fracture toughness is used to measure the viscosity dissipation. There are

$$\varepsilon = \frac{2K_{IC}}{E'}\sqrt{\frac{\pi}{l_0}},\quad \boldsymbol{P} = \frac{K_{IC}}{2}\sqrt{\frac{\pi}{l_0}} \quad \text{and} \quad T = \frac{2\sqrt{\pi}K_{IC}l_0^{3/2}}{q_0E'} \tag{22}$$

and the other two dimensionless quantities are

$$\widetilde{C} = \frac{q_0^n C' E'^{2n+1} l_0^{1-n}}{2^{2n}\pi^{n+1}K_{IC}^{2n+2}} \quad \text{and} \quad \widetilde{Q} = \frac{(1-2\nu)K_{IC}}{(1-\nu)E'}\sqrt{\frac{\pi}{l_0}} \tag{23}$$

It is evident that there exists the self-similar solution for $\widetilde{Q}\to 0$ and $n=1$ for the dimensionless parameters being independent of geometrical variables [25–27]. Substituting the boundary-condition equations into the governing equations and using the normalization scheme, one obtains

$$\widetilde{t} = \widetilde{l}(\widetilde{t})\int_0^1 \widetilde{w}(\widetilde{\zeta},\widetilde{t})\mathrm{d}\widetilde{\zeta} \tag{24}$$

$$\frac{\partial\widetilde{p}(\widetilde{x}_1,\widetilde{t})}{\partial\widetilde{x}_1}[\widetilde{w}(\widetilde{x}_1,\widetilde{t})]^{2n+1} = -\widetilde{C}\widetilde{l}(\widetilde{t})\left\{\int_{\widetilde{x}_1}^1\left[\widetilde{l}(\widetilde{t})\frac{\partial\widetilde{w}(\widetilde{x}_1,\widetilde{t})}{\partial\widetilde{t}} - \widetilde{l}'(\widetilde{t})\widetilde{x}_1\frac{\partial\widetilde{w}(\widetilde{x}_1,\widetilde{t})}{\partial\widetilde{x}_1}\right]\mathrm{d}\widetilde{\zeta}\right\}^n \tag{25}$$

$$\widetilde{w}(\widetilde{x}_1,\widetilde{t}) = \frac{2}{\pi}\widetilde{l}(\widetilde{t})\int_0^1\widetilde{p}(\widetilde{\zeta},\widetilde{t})\ln\frac{\sqrt{1-\widetilde{x}_1^2}+\sqrt{1-\widetilde{\zeta}^2}}{\sqrt{|\widetilde{x}_1^2-\widetilde{\zeta}^2|}}\mathrm{d}\widetilde{\zeta} + \widetilde{Q}\int_{\widetilde{x}_1}^1\widetilde{w}(\widetilde{\zeta},\widetilde{t})\frac{\partial\widetilde{p}(\widetilde{\zeta},\widetilde{t})}{\partial\widetilde{\zeta}}\mathrm{d}\widetilde{\zeta} \tag{26}$$

$$\sqrt{\widetilde{l}(\widetilde{t})}\int_0^1\frac{\widetilde{p}(\widetilde{\zeta},\widetilde{t})}{\sqrt{1-\widetilde{\zeta}^2}}\mathrm{d}\widetilde{\zeta} + \frac{\pi\widetilde{Q}\widetilde{\tau}_0}{2} = 1 \tag{27}$$

with the initial condition being $\widetilde{l}(\widetilde{t}_0)=1$ and $\widetilde{\tau}_0 = \lim_{x_1\to 1^-}\sqrt{1-\widetilde{x}_1^2}\widetilde{\tau}(\widetilde{x}_1,\widetilde{t})$. $\widetilde{t}_0$ is unknown and determined by Eq. (24). Here, no backflow was assumed in the derivation of Eq. (25) so that the absolute sign and signum function are removed. With the condition of no backflow, the flow rate does not change its sign at any position of the crack. This assumption is valid when the crack grows steadily and the effect of initial condition are negligible. Substituting Eq. (22) into Eq. (3) yields the normalized shear stress.

3.1.2. Asymptotic solution

In the toughness-dominant regime, asymptotic solution can be obtained using perturbation analysis for a Newtonian fracturing fluid. In this regime, the viscosity dissipation rate is much smaller than the energy release rate due to the crack propagation, $\widetilde{C}$ is therefore very small. The dependent variables were expanded in terms of $\widetilde{C}$,

$$\begin{cases}\widetilde{l}(\widetilde{t}) = \widetilde{l}_0(\widetilde{t}) + \widetilde{C}\widetilde{l}_1(\widetilde{t}) + \widetilde{C}^2\widetilde{l}_2(\widetilde{t}) + \cdots\\ \widetilde{w}(\widetilde{x}_1,\widetilde{t}) = \widetilde{w}_0(\widetilde{x}_1,\widetilde{t}) + \widetilde{C}\widetilde{w}_1(\widetilde{x}_1,\widetilde{t}) + \widetilde{C}^2\widetilde{w}_2(\widetilde{x}_1,\widetilde{t}) + \cdots\\ \widetilde{p}(\widetilde{x}_1,\widetilde{t}) = \widetilde{p}_0(\widetilde{t}) + \widetilde{C}\widetilde{p}_1(\widetilde{x}_1,\widetilde{t}) + \widetilde{C}^2\widetilde{p}_2(\widetilde{x}_1,\widetilde{t}) + \cdots\end{cases} \tag{28}$$

which were substituted into Eqs. (24), (26), (35) and (36) with $n=1$. The asymptotic expansions to the first two orders give

$$\widetilde{l}_0(\widetilde{t}) = 2^{2/3}\widetilde{t}^{\frac{2}{3}},\ \widetilde{w}_0(\widetilde{x}_1,\widetilde{t}) = 2^{4/3}\widetilde{t}^{\frac{1}{3}}\sqrt{1-\widetilde{x}_1^2} \quad \text{and} \quad \widetilde{p}_0(\widetilde{x}_1,\widetilde{t}) = \frac{2^{2/3}}{\pi}\widetilde{t}^{-\frac{1}{3}} \tag{29}$$

and

$$\begin{cases}\widetilde{l}_1(\widetilde{t}) = \left[\frac{2^{5/3}\pi}{9}\int_0^1 I_2(\widetilde{x}_1)\mathrm{d}\widetilde{x}_1 - \frac{2^{2/3}7\pi^3\ln 2}{36}\right]\widetilde{t}^{\frac{2}{3}} + \left[\frac{2^{4/3}\pi^2}{36}(6\ln 2+1) + \frac{2^{5/3}}{3}\widetilde{\tau}_0\right]\widetilde{Q}\widetilde{t}^{\frac{1}{3}}\\ \widetilde{w}_1(\widetilde{x}_1,\widetilde{t}) = \left[\frac{7\pi^2\ln 2}{36} + \frac{2^{4/3}}{9}\int_0^1 I_2(\widetilde{x}_1)\mathrm{d}\widetilde{x}_1\right]\widetilde{t}^{\frac{1}{3}}\sqrt{1-\widetilde{x}_1^2} - \frac{2^{-2/3}\pi}{3}\widetilde{t}^{\frac{1}{3}}I_2(\widetilde{x}_1)\\ \qquad + \widetilde{Q}\left[\frac{\pi}{9}(3\ln 2-1) - \frac{2^{7/3}\pi}{3}\widetilde{\tau}_0\widetilde{t}^{\frac{1}{3}}\right]\sqrt{1-\widetilde{x}_1^2} - \frac{\pi}{2}\widetilde{Q}I_1(\widetilde{x}_1)\\ \widetilde{p}_1(\widetilde{x}_1,\widetilde{t}) = \left[\frac{2^{5/3}7\pi^2\ln 2}{36} - \frac{2^{2/3}}{9}\int_0^1 I_2(\widetilde{x}_1)\mathrm{d}\widetilde{x}_1\right]\widetilde{t}^{-\frac{1}{3}} - \left[\frac{2^{1/3}\pi}{36}(6\ln 2+1) + \frac{2^{8/3}}{3}\widetilde{\tau}_0\widetilde{t}^{\frac{1}{3}}\right]\widetilde{Q}\widetilde{t}^{-\frac{2}{3}}\\ \qquad - \frac{2^{2/3}\pi^2}{24}\left[\frac{3\widetilde{x}_1\arccos\widetilde{x}_1}{\sqrt{1-\widetilde{x}_1^2}} - 2\ln(1-\widetilde{x}_1^2)\right]\widetilde{t}^{-\frac{1}{3}}\end{cases} \tag{30}$$

with

$$I_1(\widetilde{x}_1) = \int_{\widetilde{x}_1}^1 \frac{\arccos\widetilde{\zeta}\,\mathrm{d}\widetilde{\zeta}}{1-\widetilde{\zeta}^2} \tag{31}$$

$$I_2(\widetilde{x}_1) = \int_0^1 \left[\frac{3\widetilde{\zeta}\,\arccos\widetilde{\zeta}}{\sqrt{1-\widetilde{\zeta}^2}} - 2\ln(1-\widetilde{\zeta}^2)\right] \ln\frac{\sqrt{1-\widetilde{x}_1^2}+\sqrt{1-\widetilde{\zeta}^2}}{\sqrt{|\widetilde{x}_1^2-\widetilde{\zeta}^2|}}\mathrm{d}\widetilde{\zeta} \tag{32}$$

Here, $\widetilde{\tau}_0 = -\pi^2/3$. There is only one dimensionless parameter, $\widetilde{Q}$ in the asymptotic expansions. The zeroth-order asymptotic expansion represents a crack driven by an inviscid fluid, and the corresponding results are the same as those from the pressure-only model. The effect of the shear stress is present in the first-order asymptotic expansion, in which the pressure is expressed as $\ln(1-\widetilde{x}_1^2)$ in accord with the toughness scaling [11].

Let $\widetilde{Q}=0$, Eqs. (29) and (30) degenerate to the asymptotic solution of the pressure-only model. According to the first-order asymptotic expansion, the effect of the viscous dissipation consists of the pressure drop and the shear stress, while the pressure-only model considers the contribution of the pressure drop only. The pressure drop causes the decrease of the crack length, increases the crack opening and the pressure at the crack center.

The effects of shear stress are two folds according to the first-order asymptotic expansion. The terms containing $\widetilde{\tau}_0$ represent the effect of shear stress on the crack propagation criterion, and the other terms containing $\widetilde{Q}$ represent the effects of shear stress on the crack opening. The former takes effect at a large $\widetilde{t}$, leading to a higher pressure, a wider crack opening and finally a longer crack. This effect passes from Eq. (27) to Eq. (26) and finally to Eq. (24). The latter dominates at a small $\widetilde{t}$, and results in an opposite effect. This effect passes from Eq. (26) to Eq. (24) and finally to Eq. (27). Negative crack opening can be detected for a small $\widetilde{t}$ and $\widetilde{Q} >> 1$, which is in accord with results in references of [6,7]. Although the crack-closure phenomenon exists mathematically, it is hardly to find a situation where $\widetilde{Q} >> 1$ in the toughness-dominant regime according to Eq. (23).

3.2. In viscosity-dominant regime

3.2.1. Normalization

In the viscosity-dominant regime, the viscous dissipation is used to measure the fracturing toughness. There are

$$\varepsilon = \left(\frac{4q_0^{\,n}C'}{E'l_0^{2n}}\right)^{1/(2n+2)}, \quad \boldsymbol{P} = \left(\frac{q_0^{\,n}C'E'^{2n+1}}{4^{2n+1}l_0^{2n}}\right)^{1/(2n+2)} \quad \text{and} \quad T = \left(\frac{4C'l_0^{2n+4}}{q_0^{n+2}E'}\right)^{1/(2n+2)} \tag{33}$$

with two dimensionless quantities,

$$\widetilde{K}_{\mathrm{IC}} = K_{\mathrm{IC}}\left(\frac{4^n\pi^{n+1}l_0^{n-1}}{E'^{2n+1}q_0^{\,n}C'}\right)^{1/(2n+2)} \quad \text{and} \quad \widetilde{Q} = \frac{1-2\nu}{2(1-\nu)}\left(\frac{4q_0^{\,n}C'}{E'l_0^{2n}}\right)^{1/(2n+2)} \tag{34}$$

The governing equations are the same as those in the viscosity-dominant regime except for Eqs. (25) and (27), which are replaced by the following equations

$$\frac{\partial\widetilde{p}(\widetilde{x}_1,\widetilde{t})}{\partial\widetilde{x}_1}[\widetilde{w}(\widetilde{x}_1,\widetilde{t})]^{2n+1} = -\widetilde{l}(\widetilde{t})\left\{\int_{\widetilde{x}_1}^1\left[\widetilde{l}(\widetilde{t})\frac{\partial\widetilde{w}(\widetilde{\zeta},\widetilde{t})}{\partial\widetilde{t}} - \widetilde{l}'(\widetilde{t})\widetilde{\zeta}\frac{\partial\widetilde{w}(\widetilde{\zeta},\widetilde{t})}{\partial\widetilde{\zeta}}\right]\mathrm{d}\widetilde{\zeta}\right\}^n \tag{35}$$

$$\sqrt{\widetilde{l}(\widetilde{t})}\int_0^1\frac{\widetilde{p}(\widetilde{\zeta},\widetilde{t})}{\sqrt{1-\widetilde{\zeta}^2}}\mathrm{d}\widetilde{\zeta} + \frac{\pi\widetilde{Q}}{4}\lim_{x_1\to l^-}\sqrt{1-\widetilde{x}_1^2}\,\widetilde{w}(\widetilde{x}_1,\widetilde{t})\frac{\partial\widetilde{p}(\widetilde{x}_1,\widetilde{t})}{\partial\widetilde{x}_1} \geqslant \widetilde{K}_{\mathrm{IC}} \tag{36}$$

The criterion for the crack propagation, Eq. (36), is modified to allow for the singular shear stress.

3.2.2. Numerical implementation

The stress singularities, especially in the fracturing fluid, lead to many difficulties in numerical calculations. Various efforts have been done to remove the stress singularities for pressure-only models [4,28,29]. We develop a robust numerical scheme in which a series of adaptive singular interpolation functions are used.

Here, two numerical constraints are used to ensure a finite result. First, the last term in Eq. (36) is removed, so that

$$\sqrt{\widetilde{l}(\widetilde{t})}\int_0^1\frac{\widetilde{p}(\widetilde{\zeta},\widetilde{t})}{\sqrt{1-\widetilde{\zeta}^2}}\mathrm{d}\widetilde{\zeta} \geqslant \widetilde{K}_{\mathrm{IC}} \tag{37}$$

Second, negative crack openings are eliminated with an increment of $1.1\,|\widetilde{w}_{\min}|$. The former is used to avoid an infinite value of the second term in Eq. (36), which is proportional to $\lim_{\widetilde{x}_1\to\infty}(1-\widetilde{x}_1)^{-1/3}$ in the viscosity-dominant regime [6,7]. This constraint is based on a negligible shear stress, so that the contribution of the second term in Eq. (26) is disabled automatically when the effect of shear stress is negligible. The latter is used to avoid negative crack openings due to the second term in Eq. (26). This constraint is detectable in the calculation. Both constraints make it possible to obtain a result even if there is no physical solution including the negative crack opening and the potential presence of infinite stress singularity predicted in Refs. [6,7] and in Section 3.1.

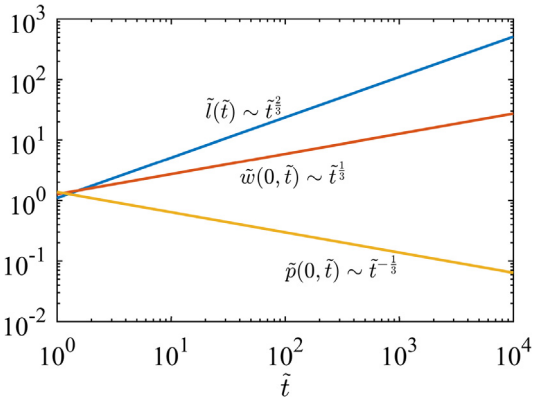

Fig. 2. Temporal evolution of the crack length, maximum crack opening and maximum pressure without fluid-lag zone for the validation of the program.

Spectral method is used to solve Eqs. (24), (35), (26) and (36). Singular basis functions are presented using the Gauss-Chebyshev interpolation. A proper numerical scheme is needed for Eq. (26). A common numerical scheme is based on the inverse of Eq. (26), and uses the crack opening as an independent variable to calculate the pressure. Such a method is likely sensitive to the initial-condition [28,29]. Here, an iterative numerical scheme is used to limit the sensitivity to initial condition. The initial crack opening and its temporal increment are determined by assuming a self-similar crack propagation, and numerical results show the error introduced by the initial conditions decreases rapidly. The pressure and the shear stress are calculated from Reynolds' equation with the crack propagation criterion. The integral equation is used to calculate the crack opening, and the mass conservation is used to find the crack length. The numerical calculation is terminated when the maximum relative error of the crack opening is less than a pre-determined value. Implicit Euler method is used for the time integration, and adaptive time step is used to improve the calculation. The details of the numerical scheme are given in Appendix B.

A pressure-only calculation was performed to validate the program for the numerical analysis. For a Newtonian fracturing fluid, the problem is self-similar, and the crack length, maximum crack opening and maximum pressure are power-law functions of time, with the power indexes being 2/3, 1/3 and $-1/3$, respectively [11]. Fig. 2 shows the numerical results, which are in accord with the analytical solution, and the relative errors of the power indexes are less than 0.3%. There is no mesh-dependent result for the pressure-only model, and the two numerical constraints do not take effect.

3.2.3. Crack-closure phenomenon

Mesh-dependent phenomenon is obtained with the developed numerical scheme. Fig. 3 shows temporal evolution of both the crack length and the crack opening, which are mesh-dependent, for $\widetilde{K}_{IC} = 0$, $\widetilde{Q} = 1$ and $n = 1$ in the early time of hydraulic fracturing. It is evident that the results are mesh-independent for large time. The second numerical constraint takes effect at small times when the numerical results are mesh-dependent. Note that the crack growth of pressure-only model is self-similar, and the numerical results are mesh-independent. The mesh-dependent phenomenon is due to the shear stress, which fails the first constraint of negligible shear stress. Consequently, the effect of shear stress is dominant at small times and becomes negligible at large times. There is a criterion for the occurrence of mesh-dependent phenomenon, suggesting the dominant effect of shear stress. It is rational to conclude that the

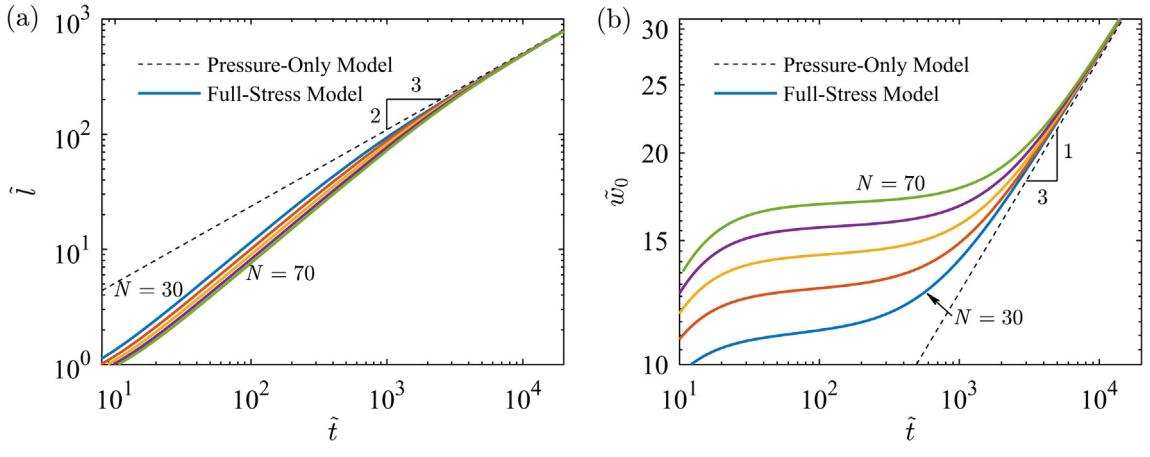

Fig. 3. Mesh-dependent results of (a) crack length, and (b) crack opening at the wellbore.

mesh-dependent results are due to the crack-closure phenomenon induced by shear stress at small times, as shown in Refs. [6,7] and in Section 3.1. The mesh-dependent criterion is therefore a necessary condition for the crack closure.

There is a critical minimum mesh length for the presence of a mesh-dependent result. As discussed above, the crack opening consists of the contribution from both the pressure and the shear stress. The numerical calculation gives the asymptotic solution of the crack opening near the crack tip as

$$\widetilde{w}(\widetilde{x}_1,\ \widetilde{t}\ ) = \widetilde{w}_{\mathrm{p}} + \widetilde{w}_{\mathrm{t}} \simeq -\frac{e_{\mathrm{p}}(e_{\mathrm{p}}+4)\Gamma(1/2+e_{\mathrm{p}})\widetilde{p}_0}{5(2e_{\mathrm{p}}+1)\ \Gamma(1+e_{\mathrm{p}})}(1-\widetilde{x}^2)^{e_{\mathrm{p}}+1} + \frac{\widetilde{Q}\widetilde{\tau}_0}{2(e_{\mathrm{t}}+1)}(1-\widetilde{x}^2)^{e_{\mathrm{t}}+1} \tag{38}$$

for $\widetilde{p} \simeq \widetilde{p}_0[1-\sqrt{\pi}\ \ \Gamma(1+e_{\mathrm{p}})/\Gamma(1/2+e_{\mathrm{p}})(1-\widetilde{x}_1^2)^{e_{\mathrm{p}}}]$ and $\widetilde{\tau} \simeq \widetilde{\tau}_0(1-\widetilde{x}_1^2)^{e_{\mathrm{t}}}$, where $\widetilde{p}_0 > 0$, $\widetilde{\tau}_0 < 0$, $-1/2 < e_{\mathrm{p}} < 0$ and $-1 < e_{\mathrm{t}} < 0$. The relative error of the coefficient of $\widetilde{w}_{\mathrm{p}}$ is less than 4% for $e_{\mathrm{p}} > -0.1$. With $e_{\mathrm{p}} > e_{\mathrm{t}}$, there is no crack closure only for $\widetilde{\tau}_0 << \widetilde{p}_0$, and the near-crack-tip mesh size is too large to reveal any possible negative crack opening for large $\widetilde{t}$. There is a critical length of $\Delta\widetilde{x}_{\mathrm{cr}}$ for a constant $\widetilde{Q}$, and a mesh-dependent result is obtained when the mesh size near the crack tip is smaller than $\Delta\widetilde{x}_{\mathrm{cr}}$; equivalently, there exists a critical $\widetilde{Q}$ for a constant $\Delta\widetilde{x}$.

The critical $\widetilde{Q}$ is estimated as below. For a constant mesh size near the crack tip, increasing $\widetilde{Q}$ from a sufficiently small value to the critical value leads to the presence of the crack closure. A small value of $\widetilde{Q}$ has a negligible effect on the crack opening, and the asymptotic solution of the crack opening can be obtained with $\widetilde{Q}=0$. The shear stress and $\widetilde{w}_{\mathrm{T}}$ are calculated by using the asymptotic solution. Assume that $\widetilde{Q}=0$ is valid before the onset of the crack closure. The $\widetilde{Q}_{\mathrm{cr}}$ is calculated with $\widetilde{w}_{\mathrm{p}} = \widetilde{w}_{\mathrm{t}}$ at the mesh point near the crack tip. For a constant $\widetilde{Q}$, substituting Eq. (38) into Eqs. (24)–(27) yields the $\Delta\widetilde{x}_{\mathrm{cr}}$ as

$$\Delta\widetilde{x}_{\mathrm{cr}} = \left[\frac{25(n+2)^{2n}\widetilde{Q}^{n+2}}{2^{4n}\pi(3n+8)^2(2-n)}\right]^{\frac{1}{n}} \tag{39}$$

For Newtonian fracturing fluid, Eq. (39) gives $\Delta\widetilde{x}_{\mathrm{cr}} \approx 0.037\widetilde{Q}^3$. It is evident that $\Delta\widetilde{x}_{\mathrm{cr}}$ is very sensitive to $\widetilde{Q}$, and it is very difficult to reveal the crack closure for $\widetilde{Q} < 0.01$.

Numerical calculations are conducted with a constant minimum mesh size near the crack tip. $\Delta\widetilde{x}_{\mathrm{cr}}$ is calculated with the relative error of the crack length being $\sim$5% between $N=30$ and $N=70$, and a larger $\Delta\widetilde{x}_{\mathrm{cr}}$ can be obtained for a smaller critical relative error. Fig. 4 shows the critical mesh size of the mesh near the crack tip for the crack closure. The estimated $\Delta\widetilde{x}_{\mathrm{cr}}$ is much smaller than the numerical value. Thus, Eq. (39) is very conservative to determine whether there exists the crack closure, and reveals a power-law relationship between the critical mesh length and $\widetilde{Q}$. From the numerical calculations, an empirical criterion is obtained as

$$\Delta\widetilde{x}_{\mathrm{cr}} = (0.1421n^2 - 0.1369n + 0.0323)\widetilde{Q}^{\frac{n+1}{n}} \tag{40}$$

which is valid for the relative error of the crack length being less than 5%.

3.2.4. Energy analysis: the shear-stress-dominant regime

All of the powers in Eqs. (17)–(20) are normalized with q_0P, which is defined in Eqs.(22). For pressure-only problems without fluid-lag zone, the scaling laws of the powers (energy rates), which represent the temporal evolutions of powers, can be calculated by using the scaling laws of the crack length, the crack opening and the pressure. The power-law relationships are $\widetilde{\eta}_{\mathrm{tot}}\widetilde{t}^{-n/(n+2)}$, $\widetilde{\eta}_{\mathrm{visc}}\widetilde{t}^{-n/(n+2)}$ and $\widetilde{\eta}_{\mathrm{frac}}\widetilde{t}^{-1/(n+2)}$ [11], which are valid in the viscosity-dominant regime. For shear thinning fracturing fluid, the ratio of the viscous dissipation to the fracturing energy increases with the increase of time, the viscous dissipation is dominant for large times, and the fracturing energy is dominant for small time. For a shear thickening fracturing fluid, the fracturing work is dominant for large time. For a Newtonian fracturing fluid, the problem is self-similar during hydraulic fracturing.

For the full-stress model, it is impossible to calculate the powers for the early stage due to the mesh-dependent behavior. As shown in Fig. 5, the full-stress model degenerates to the pressure-only model for large times, and the exponents of the power-law relationships are in accord with the analytical value of $-1/3$. For small times, the exponents of the pressure-only model are constant,

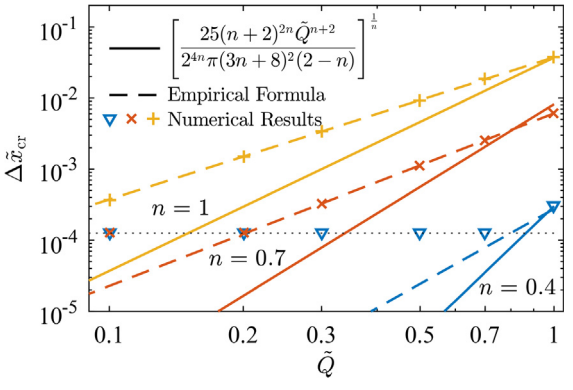

Fig. 4. Critical mesh size for the mesh near crack tip for crack closure (Solid lines are the estimated value, and the dot line is the minimum mesh size used in numerical calculation.)

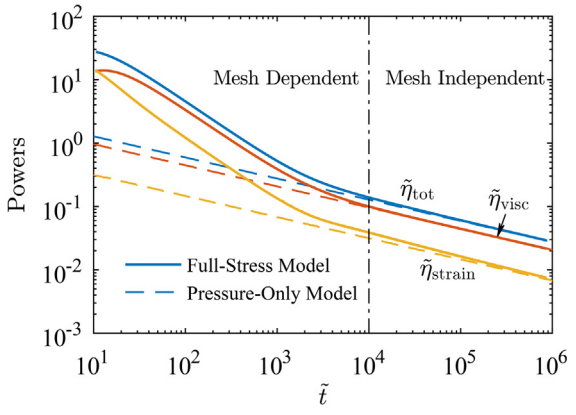

Fig. 5. Variation of energy dissipation rates with time for $\widetilde{K}_{\rm IC} = 0$, $\widetilde{Q} = 1$ and $n = 1$ (Dashed lines represent the pressure-only model, and solid lines represent the full-stress model.)

which indicates no dominant-regime transition. The mesh-dependent behavior of the full-stress model reveals that the viscosity-dominant regime is different from the shear-stress-dominant regime in accord with the scaling analysis.

3.3. Effect of lubrication theory

A method for eliminating the stress singularity in a fracturing fluid is to use the theory of two-dimensional flow [15]. The vertical component of the fluid velocity is not negligible near the crack tip. In their work [15], Bui and Parnes used potential flow in an elliptical fluid channel, leading to a non-singular pressure at the crack tip. Currently, two-dimensional flow has not been widely accepted; however, two-dimensional flow plays a great role at the tip of the fluid flow. The assumption of the elliptical crack profile is not necessary due to the process zone with the crack opening being $O[(l - x_1)^{3/2}]$ [14]. Here, both elliptical and sharper crack profiles are used as the fluid channel in the numerical analysis, and the fracturing fluid is Newtonian.

Analyzing the viscous flow in the channel between crack surfaces is a challenging task. The solution needs to be of high precision to capture the details near the crack tip, and the crack opening is about 3 to 5 orders of magnitude smaller than the crack length. A numerical simulation involving in the complete crack is not preferred. Note that this subsection aims at presenting the critical length for a negligible effect of the vertical velocity, so that the lubrication theory is applicable if the distance from the fluid tip is larger than this critical length. The crack tip is therefore enlarged to capture the details of the flow. A moving coordinate system, which is attached to the crack tip with a constant velocity of V, as shown in Fig. 6. The crack profile is expressed as $b \times f(X_1/a)$ where a and b are the length and width of the crack, respectively, and $f(x) = |x|^{e_{\rm w}}/2$, where $e_{\rm w}$ is the constant power-law index of crack opening. A large value of b/a will enlarge the crack.

The flow of the fracturing fluid in the crack satisfies the Stokes equation

$$\mathbf{0} = -\nabla p + \mu \Delta \boldsymbol{v} \tag{41}$$

with μ being the dynamic viscosity, $\nabla = \boldsymbol{e}_i \partial_i$ and $\Delta = \partial_{kk}$. Non-slip boundary conditions are used on the crack surfaces as

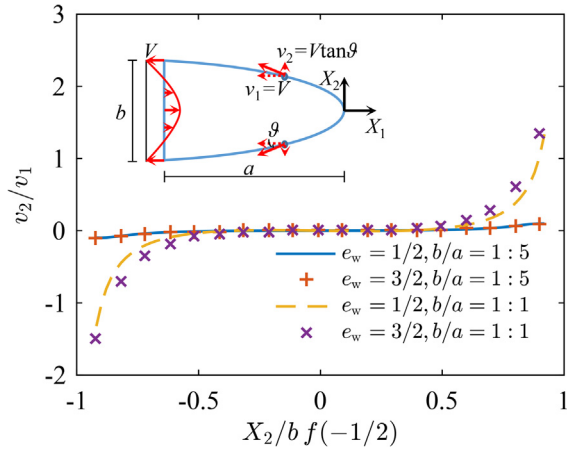

Fig. 6. Ratio of v_2 to v_1 at $X_1 = -a/2$ ($e_{\rm w} = 1/2$ corresponds to an elliptical crack, and $e_{\rm w} = 3/2$ corresponds to the crack-tip region with a process zone. A larger value of b/a represents a higher-level enlargement of the crack tip.)

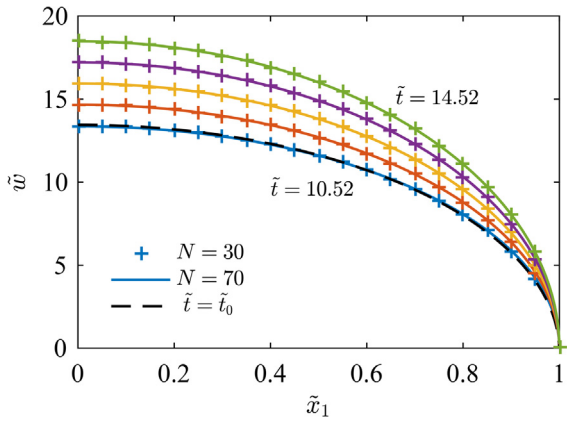

Fig. 7. Temporal evolution of the crack opening of a slit crack during hydraulic fracturing with $\widetilde{Q} = 1$ without the crack propagation.

$$v_1 = -V \quad \text{and} \quad v_2 = (b/a)f'(X_1/a)V \tag{42}$$

for the upper crack surface. The velocity of the lower crack surface is obtained by using the symmetric characteristic of the problem. At the entrance of the fluid channel, the velocity is approximated as

$$v_1 = \left[\frac{3}{4}\left(1 - \frac{2X_2}{b}\right)^2 - 1\right]V \quad \text{and} \quad v_2 = \frac{2X_2}{a}f'(-1)V \tag{43}$$

where v_1 is used to ensure the mass conservation. Note that an alternative boundary condition at the entrance is the surface traction which limits the constant stress discrepancy introduced by Eqs.(43). Eqs. (41)–(43) are solved by BEM with quadratic isoparametric discontinuous boundary elements [30].

Fig. 6 shows the ratio of the vertical component of the velocity to the horizontal component of the velocity on the cross section of an elliptical crack profile or a slit crack with a process zone. The numerical simulation was performed for $b/a = 1/5$ and $b/a = 1$; the one with $b/a = 1$ represents a greater enlargement of the crack-tip region. The ratio was calculated on the cross section of the crack at $X_1 = -a/2$. A small ratio was obtained for the cross section being far away from the crack tip. There must be a critical distance for the velocity ratio being negligible, and the lubrication theory is valid in the region with a distance being larger than the critical distance. The critical distance is comparable to the crack opening, which is much smaller than the crack length. In the viscosity-dominant regime, the effect of the pressure at the near-tip region on the crack propagation criterion is negligible because the stress singularity is integrable. Hence, the effect of lubrication theory on the crack-closure phenomenon is negligible.

3.4. Discussion on the full-stress model without fluid-lag zone

The mesh-dependent results were obtained for the crack opening due to the shear stress. Fig. 7 shows the reopening of the crack with continuous injection of the fracturing fluid after the crack closure in the fluid-tip region. In the numerical calculation, the crack length remains unchanged, and the crack opening changes with the interaction between the pressure and the shear stress. The mesh-dependent results were used as the initial conditions for a slit crack in the numerical calculation with $\widetilde{t}_0 \approx 10.52$, and the time step being limited up to 1% of the total time. The continuous flow of the fracturing fluid enlarges the crack opening and increases the possibility for the crack to propagate. The crack regains the ability to propagate when the stress intensity factor is larger than the fracture toughness. The result shows that the stress intensity factor increases greatly at the onset of the reopening.

4. Hydraulic fracture with a fluid-lag zone

The presence of a fluid-lag zone at the crack tip eliminates the stress singularity in the viscous fracturing fluid, which is essential to the asymptotic analysis of crack-closure phenomenon [6,7]. For the pressure-only model, the crustal stress reduces the size of the fluid-lag zone [29]. The following analysis is focused on if the fluid-lag zone can introduce crack-closure phenomenon in the fluid-tip region.

4.1. Scaling analysis

Hydraulic fracturing is an initial-boundary value problem and can be expressed mathematically as

$$\begin{Bmatrix} l \\ l_f \\ w \\ p \end{Bmatrix} = \boldsymbol{f}\left(x_1,\, t;\, C',\, n,\, E',\, \nu,\, K_{\mathrm{IC}},\, \gamma\cos\theta;\, q_0,\, p_{\mathrm{v}},\, \sigma_\infty;\, l_{\mathrm{f0}}\right) \tag{44}$$

The shear stress is not included in Eq. (44) because it is related to the crack opening and the pressure in Eq. (3). In the scaling analysis, the system starts from infinitesimal to infinity in the parameter space, and the crack profile is self-similar [27]. Thus, the initial-condition of Eq. (9) is not needed.

We introduce the following transformations,

$$l(t) = L(t)L_{\mathrm{f}}(t),\ w(x_1, t) = W(t)\widetilde{w}(\widetilde{x}_1) \quad \text{and} \quad p(x_1, t) - p_{\mathrm{v}} = \mathbf{\Sigma}(t)\widetilde{p}(\widetilde{x}_1) \tag{45}$$

where $L(t)$, $L_{\mathrm{f}}(t)$, $W(t)$ and $\mathbf{\Sigma}(t)$ are of either power-laws or exponentials, corresponding to the power-law and exponential boundary conditions, respectively. Equation is used to find the zero-order asymptotic solution with respect to time for $l_{\mathrm{f}}(t) = L_{\mathrm{f}}(t)$. Here, transformations for the power-law type are used, and there are seven dimensionless quantities as,

$$\begin{aligned}
&\mathscr{V} = \frac{q_0 t}{W(t)L_{\mathrm{f}}(t)}, \quad \mathscr{P} = \frac{4\Sigma(t)L_{\mathrm{f}}(t)}{W(t)E'}, \quad \mathscr{M} = \frac{C'\dot{W}^n(t)L_{\mathrm{f}}^{n+1}(t)}{\Sigma(t)W^{2n+1}(t)}, \quad \mathscr{K} = \frac{K_{\mathrm{IC}}}{2\Sigma(t)}\sqrt{\frac{\pi L(t)}{L_{\mathrm{f}}(t)}},\\
&\mathscr{Q} = \frac{2(1-2\nu)\Sigma(t)}{(1-\nu)E'}, \quad \mathscr{S} = \frac{4(\sigma_\infty + p_{\mathrm{v}})L_{\mathrm{f}}(t)}{W(t)E'} \quad \text{and} \quad \mathscr{R} = -\frac{\gamma\cos\theta}{\Sigma(t)W(t)}
\end{aligned} \tag{46}$$

where $\mathscr{V}$, $\mathscr{P}$, $\mathscr{M}$, $\mathscr{K}$, $\mathscr{Q}$, $\mathscr{S}$ and $\mathscr{R}$ are the dimensionless volume of the fluid channel between the crack surfaces, the crack opening due to the pressure, the viscous dissipation, the fracture toughness, the crack opening due to the shear stress, the crustal stress, and the surface tension, respectively. The effect of wettability is represented by $\mathscr{R}$, in which $W(t)$ is the characteristic wellbore crack opening and the surface tension is at the fluid tip.

It is of great importance to use proper dimensionless quantities to simplify the equations. Similar to the derivation of Eq. (33), the mass conservation is preserved, the pressure-induced crack opening is used to measure the overall crack opening, and the energy of crack propagation is used to measure that of viscous dissipation. In the stage where the fluid-lag zone is very large, the length of the fluid channel is much shorter than the crack length. The length of the fluid-lag zone decreases under the action of the crustal stress [29], indicating that the change of stress intensity factor caused by crustal stress is comparable to that induced by the pressure. Because the fracture toughness is constant and negligible in the viscosity-dominant regime, it is rational to assume that the stress intensity factor due to the pressure is equivalent to that due to the crustal stress, and $\mathscr{S}$ is therefore used. Eliminating the four dimensionless quantities, $\mathscr{V}$, $\mathscr{P}$, $\mathscr{M}$ and $\mathscr{S}$, we obtain the scaling laws and other dimensionless quantities as

$$\begin{aligned}
&L(t) = \frac{1}{\sigma_\infty + p_{\mathrm{v}}}\left(\frac{C'E'^{n+1}}{4^{n+1}t^n}\right)^{\frac{1}{n+2}}, \quad L_{\mathrm{f}}(t) = \left[\frac{(n+2)^n E' q_0^{n+2} t^{2(n+1)}}{4C'}\right]^{\frac{1}{2n+4}},\\
&W(t) = \left[\frac{4C' q_0^{n+2} t^2}{(n+2)^n E'}\right]^{\frac{1}{2n+4}} \quad \text{and} \quad \Sigma(t) = \left(\frac{C'E'^{n+1}}{4^{n+1}t^n}\right)^{\frac{1}{n+2}}
\end{aligned} \tag{47}$$

$$\begin{aligned}
&\mathscr{Q} = \frac{1-2\nu}{1-\nu}\left[\frac{C'}{2^n(n+2)^n E' t^n}\right]^{\frac{1}{n+2}}, \ \mathscr{K} = \frac{\frac{1}{\pi\sqrt{2}}K_{\mathrm{IC}}}{2(\sigma_\infty + p_{\mathrm{v}})^{1/2}}\left[\frac{4^{2n+3}(n+2)^n}{q_0^{n+2}C'^{2n+3}E'^3 t^2}\right]^{\frac{1}{4n+8}}\\
&\text{and} \quad \mathscr{R} = -\left\{\frac{4^{2n+1}(n+2)^n t^{2(n-1)}}{C'^3 E'^{2n+1} q_0^{n+2}}\right\}^{\frac{1}{2n+4}}\gamma\cos\theta
\end{aligned} \tag{48}$$

Note that the scaling laws are approximate because there is $L(t)$ in the integral equations of the crack opening and the stress intensity factor. In Eq. (48), the dimensionless quantities $\mathscr{Q}$, $\mathscr{K}$ and $\mathscr{R}$ represent the ratio of the crack opening due to the shear stress to that due to the pressure, the ratio of fracture toughness to the combined effects of the crustal stress and the viscous dissipation, and the ratio of surface tension to the combined effects of the pressure and the viscous dissipation. Both $\mathscr{Q}$ and $\mathscr{K}$ are decreasing functions of time, so both the shear stress and the fracture toughness are negligible at large times in comparison with the pressure and the viscosity, respectively. If there is the crack closure in the fluid-tip region or deflection, it occurs at a small time. This analysis demonstrates a key point that the viscosity-dominant regime is different from the shear-stress-dominant regime. $\mathscr{R}$ is a decreasing function of time and negligible at large times for a shear thinning fracturing fluid, is an increasing function of time and is dominant at large times for a shear thickening fracturing fluid, and is constant for a Newtonian fracturing fluid.

4.2. Numerical implementation

Similar to the normalization scheme in Section 3.1, we use the following normalization scheme

$$x_1 = l_{\mathrm{f0}}\widetilde{l}_{\mathrm{f}}(\widetilde{t})\widetilde{x}_1,\ w(x_1, t) = \varepsilon l_{\mathrm{f0}}\widetilde{w}(\widetilde{x}_1, \widetilde{t}),\ p(x_1, t) - p_{\mathrm{v}} = \boldsymbol{P}\widetilde{p}(\widetilde{x}_1, \widetilde{t}),\ t = T\widetilde{t} \tag{49}$$

with the crack length being normalized by $l_{\mathrm{f0}}\widetilde{l}_{\mathrm{f}}(\widetilde{t})$. Either the initial crack length or the initial fluid-tip position can be included in the unit system. The initial fluid-tip position is used to take into account the effect of the viscous dissipation. In the viscosity-dominant regime, there are

$$\varepsilon = \left(\frac{4q_0^n C'}{E' l_{\mathrm{f0}}^{2n}}\right)^{1/(2n+2)}, \quad \boldsymbol{P} = \left(\frac{E'^{2n+1} q_0^n C'}{4^{2n+1} l_{\mathrm{f0}}^{2n}}\right)^{1/(2n+2)}, \quad T = \left(\frac{4C' l_{\mathrm{f0}}^{2n+4}}{q_0^{n+2}E'}\right)^{1/(2n+2)} \tag{50}$$

with the dimensionless parameters as

$$\widetilde{K}_{\mathrm{IC}} = K_{\mathrm{IC}}\left(\frac{4^n\pi^{n+1}l_{\mathrm{f0}}^{n-1}}{E'^{2n+1}q_0^nC'}\right)^{1/(2n+2)},\quad \widetilde{Q} = \frac{1-2\nu}{2(1-\nu)}\left(\frac{4q_0^nC'}{E'l_{\mathrm{f0}}^{2n}}\right)^{1/(2n+2)},$$
$$\widetilde{\sigma}_\infty = (\sigma_\infty + p_{\mathrm{v}})\left(\frac{4^{2n+1}l_{\mathrm{f0}}^{2n}}{q_0^nC'E'^{2n+1}}\right)^{1/(2n+2)},\quad \widetilde{\gamma} = -\frac{\gamma\cos\theta}{(q_0^nC'E'^nl_{\mathrm{f0}}^{1-n}/4^n)^{1/(n+1)}}\ \text{and}\ n \tag{51}$$

where $\widetilde{\sigma}_\infty$ is the dimensionless crustal stress, and $\widetilde{\gamma}$ is the dimensionless surface tension. It is evident that the effect of the crustal stress is dependent on the position of the fluid tip, and the effect of the surface tension is dependent on the flow behavior index in accord with the scaling analysis. With the dimensionless parameters and the assumption of no backflow, Eqs. (1) –(9) become

$$\widetilde{t} = \widetilde{l}_{\mathrm{f}}(\widetilde{t})\int_0^1 \widetilde{w}(\widetilde{\zeta},\widetilde{t})\mathrm{d}\widetilde{\zeta} \tag{52}$$

$$\widetilde{q}(\widetilde{x}_1,\widetilde{t}) = 1 - \int_0^{\widetilde{x}_1}\left[\widetilde{l}_{\mathrm{f}}(\widetilde{t})\frac{\partial\widetilde{w}(\widetilde{\zeta},\widetilde{t})}{\partial\widetilde{t}} + \widetilde{l}'_{\mathrm{f}}(\widetilde{t})\widetilde{w}(\widetilde{\zeta},\widetilde{t})\right]\mathrm{d}\widetilde{\zeta} + \widetilde{l}'_{\mathrm{f}}(\widetilde{t})\widetilde{x}_1\widetilde{w}(\widetilde{x}_1,\widetilde{t}) \tag{53}$$

$$\frac{\partial\widetilde{p}(\widetilde{x}_1,\widetilde{t})}{\partial\widetilde{x}_1} = -\mathrm{sgn}\{\widetilde{q}(\widetilde{x}_1,\widetilde{t})\}\widetilde{l}_{\mathrm{f}}(\widetilde{t})\frac{|\widetilde{q}(\widetilde{x}_1,\widetilde{t})|^n}{[\widetilde{w}(\widetilde{x}_1,\widetilde{t})]^{2n+1}} \tag{54}$$

$$\widetilde{w}(\widetilde{x}_1,\widetilde{t}) = \frac{2}{\pi}\widetilde{l}_{\mathrm{f}}(\widetilde{t})\int_0^1 \widetilde{p}(\widetilde{\zeta},\widetilde{t})ln\frac{\sqrt{\widetilde{l}^2(\widetilde{t}) - \widetilde{x}_1^2} + \sqrt{\widetilde{l}^2(\widetilde{t}) - \widetilde{\zeta}^2}}{\sqrt{|\widetilde{x}_1^2 - \widetilde{\zeta}^2|}}\mathrm{d}\widetilde{\zeta} + \widetilde{Q}\int_{\widetilde{x}_1}^1 \widetilde{w}(\widetilde{\zeta},\widetilde{t})\frac{\partial\widetilde{p}(\widetilde{\zeta},\widetilde{t})}{\partial\widetilde{\zeta}}\mathrm{d}\widetilde{\zeta} + \widetilde{\sigma}_\infty\widetilde{l}_{\mathrm{f}}(\widetilde{t})\sqrt{\widetilde{l}^2(\widetilde{t}) - \widetilde{x}_1^2} \tag{55}$$

$$\widetilde{K}_{\mathrm{IC}} = \sqrt{\widetilde{l}_{\mathrm{f}}(\widetilde{t})}\sqrt{\widetilde{l}(\widetilde{t})}\int_0^1 \frac{\widetilde{p}(\widetilde{\zeta},\widetilde{t})}{\sqrt{\widetilde{l}^2(\widetilde{t}) - \widetilde{\zeta}^2}}\mathrm{d}\widetilde{\zeta} + \frac{\pi}{2}\sqrt{\widetilde{l}_{\mathrm{f}}(\widetilde{t})}\sqrt{\widetilde{l}(\widetilde{t})}\widetilde{\sigma}_\infty \tag{56}$$

$$\widetilde{p}(\widetilde{l}_{\mathrm{f}}(\widetilde{t}),\widetilde{t}) = \frac{\widetilde{\gamma}}{\widetilde{w}(\widetilde{l}_{\mathrm{f}}(\widetilde{t}),\widetilde{t})} \tag{57}$$

and the initial condition becomes $\widetilde{l}_{\mathrm{f}}(\widetilde{t}_0) = 1$. For a small fluid-lag zone, the fluid tip coincides with the crack tip, and Eqs. (52)–(57) degenerate to Eqs. (24)–(27); the full-stress model with a fluid-lag zone degenerates to that without fluid-lag zone.

An adaptive mesh is used with a constant number of mesh nodes in the fluid channel and no less than 10 nodes in the fluid-lag zone. Lagrange quadrature is used, and the variable nodes coincide with the mesh nodes to reduce the error introduced by extrapolation. The implicit Eulerian method is used for the integration of time. Using two iterative loops in a single step, we can obtain the convergent result. First, the crack opening and the crack length are calculated from the previous step with Eqs. (47), and the fluid-tip position is calculated from Eq. (52). Then, the flow rate and the pressure gradient are calculated. Eq. (57) is used to determine the new crack opening. If the relative error between the newly calculated crack opening and the previously calculated one is less than the pre-given error, the inner loop ends; otherwise, the new crack opening is used for the subsequent numerical calculation. In the numerical calculation, the relaxation factor is 10^{-3}. After finishing the calculation in the inner loop, we obtain a new crack length from Eq. (47). The outer loop ends when the relative error between the two crack lengths is sufficiently small.

A comparison study has been performed to validate the numerical scheme. Fig. 8 shows the evolution of the positions of the crack tip and the fluid tip calculated from the models with and without a fluid-lag zone. The numerical calculation is focused on the pressure-only model with $\widetilde{\sigma}_\infty = -0.1$, $n = 1$, and $\widetilde{K}_{\mathrm{IC}} = 0$. For the model with a fluid-lag zone, the size of the fluid-lag zone is large at

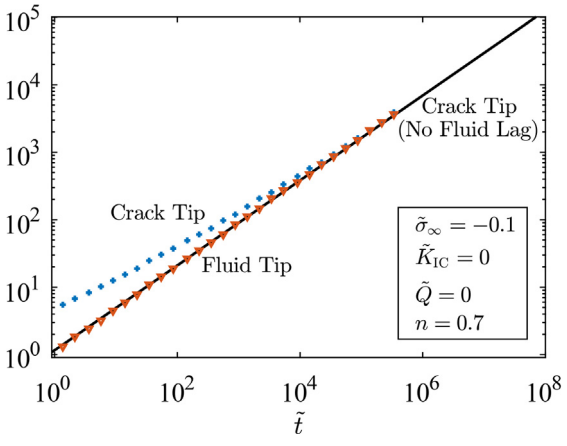

Fig. 8. Comparison between the results with and without a fluid-lag zone. The crack tip coincides with the fluid tip at large times under the crustal stress for the model with a fluid-lag zone. The model with a fluid-lag zone degenerates to the model without a fluid-lag zone at large time.

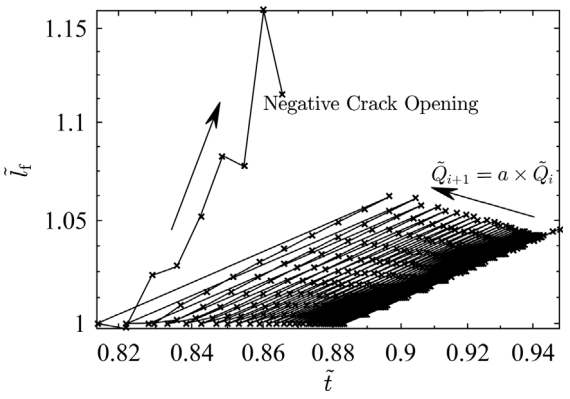

Fig. 9. Divergent result (negative crack opening) from the full-stress model with a fluid-lag zone. An iterative numerical scheme has been used. For each iteration, $\widetilde{Q}$ is increased by a multiplier.

early time, and decreases under the action of the crustal stress to a negligible value at large times, where the model with a fluid-lag zone degenerates to the model without the fluid-lag zone.

4.3. Unstable crack growth

It is very difficult to demonstrate the crack closure for the full-stress model with a fluid-lag zone because no physical solution can be obtained. The numerical calculation is divergent once crack closure occurs, and there is no further information available for the analysis. According to the model without fluid-lag zone, a mesh-dependent result is present under the following conditions of (1) $\widetilde{t} \leqslant \widetilde{t}_{\rm cr}$, which is equivalent to $\Delta\widetilde{x} \leqslant \Delta\widetilde{x}_{\rm cr}$, with certain values of $\widetilde{Q}$, and (2) $\widetilde{Q} > \widetilde{Q}_{\rm cr}$ at certain times. Two numerical schemes can be used according to the two conditions. For a constant $\widetilde{Q}$, a time reversal calculation is needed to achieve the first condition from a large time, and for a constant time, divergent results are obtained by increasing $\widetilde{Q}$ from a small value.

Hydraulic fracturing is a diffusion process [31] with phase transition. The first numerical scheme is inapplicable because the time reversal problem of a diffusion process is ill-conditioned. Here, an iterative process is used to achieve the second condition. For each iteration, the calculation starts with the same initial fluid-tip position in individual calculation. Several time steps are used to examine whether the calculation is divergent. The loop ends if a divergent result occurs; otherwise, the calculated results are mapped to the initial fluid-tip position according to Eqs. with $\widetilde{Q}$ being increased with a multiplier, and other dimensionless parameters remain unchanged.

Fig. 9 shows the divergent result of the fluid-tip position, indicating that the fluid-lag zone cannot eliminate the crack-closure phenomenon. A plausible mechanism is that the crack-closure phenomenon is due to the interaction of elastic deformation and viscous flow which is independent of the crack-tip asymptotics. From this perspective, branching near the fluid tip on the crack surfaces and away from the crack tip may appear. The other reason is likely due to the inapplicability of the lubrication theory at the fluid tip since the flow near the fluid tip is two-dimensional. Lubrication theory is invalid in the near-fluid-tip region with its length comparable with the crack opening. However, such a region is much shorter than the crack, and the lubrication theory is therefore valid.

In the calculation, the multiplier of $a = 1.05$ has been used to increase $\widetilde{Q}$ step by step. The other parameters are $\widetilde{K}_{\rm IC} = 0$, $n = 0.7$, $\widetilde{\sigma}_\infty = -0.1$, $\widetilde{\gamma} = 0$. Uniform mesh is used with 60 nodes for the fluid channel. Negative crack opening is observed for $\widetilde{Q} = 0.4$, which is slightly larger than the result of $\widetilde{Q}_{\rm cr} = 0.23$ for the model without fluid-lag zone. This value decreases with the increase of the crustal stress. The fluid-lag zone may decrease the possibility of the crack closure, which cannot be revealed precisely with the numerical scheme used in this work.

4.4. Effect of fluid-lag zone

The existence of a fluid-lag zone leads to the failure to eliminate the crustal stress by the superposition principle. The fluid surface and moving contact line appear near the front of the fracturing fluid [5]. According to Eq. (47), the dimensionless crack length decreases with time during the hydraulic fracturing. For a small fraction of fluid, the dimensionless length of the fluid-lag zone can be approximated as

$$L_{\rm lag}(t) = L(t) - 1 \approx L(t) \tag{58}$$

where $L_{\rm lag}(t) = l_{\rm lag}(t)/L_{\rm f}(t)$. The dimensionless parameter, $\mathscr{K}$, gives a characteristic time as

$$t_{\rm K} = \left(\frac{\pi K_{\rm IC}^2}{\sigma_\infty + p_{\rm v}}\right)^{n+2} \sqrt{\frac{(n+2)^n}{4 q_0^{n+2} C' E'^{2n+3}}} \tag{59}$$

which represents the characteristic time for the fluid-lag zone being negligible. For large times, the size of the fluid-lag zone can be

predicted using the Galilean transform for a Newtonian fracturing fluid [11]. Note that a large dimensionless crustal stress may introduce large error in initial condition in the numerical calculation, and increasing crustal stress is mathematically equivalent to increasing the initial time according to Eq. (51).

The problem is self-similar for Newtonian fracturing fluid if the crustal stress, the vapor pressure, the shear stress, and the wettability are negligible. The size of the fluid-lag zone increases with increasing time for shear thinning fracturing fluid and decreases for shear thickening fluid. There is a scaling law for the evolution of the fluid-lag zone. Using the transformations in Eq. (45) and equating the fracture toughness to the stress intensity factor introduced solely by the pressure, one obtains

$$L(t) = \left[\frac{q_0^{n+2} C'^3 E'^{4n+5} t^{2(1-n)}}{4^{2n+1}\pi^{2n+4}(n+2)^n K_{IC}^{4n+8}} \right]^{\frac{1}{2n+4}} \tag{60}$$

with the other scaling laws being the same as those in Eq. (47). From numerical calculations, Eq. (60) gives the same power-law exponents as the numerical results only for $n = 1$. There exist slight differences of the power-law exponents for $n \neq 1$ between the numerical results and the scaling laws due to the existence of the dimensionless crack length in the boundary integral equation and the stress intensity factor.

In general, the effects of the wettability are time-dependent. The shear-stress-dominant regime is limited to the early time of hydraulic fracturing in the case that the crack closure in the fluid-tip region may occur. A small size of the fluid-lag zone is detected due to the negative effect of the shear stress on the crack opening. According to Eq. (48), the effect of the surface tension is significant at large times for a shear thickening fracturing fluid, or at small times for a shear thinning fluid. Note that the surface tension is often neglected in the simulation and design of hydraulic fracturing because of small order of magnitude. However, the effect of wettability on the crack opening is crucial for microcracks which have large curvature [5].

4.5. Discussion on the full-stress model with a fluid-lag zone

The analysis has revealed the possible occurrence of the crack-closure phenomenon in the hydraulic fracturing with a fluid-lag zone, although it occurs more difficultly than the case without a fluid-lag zone. According to Eqs. (2) and (3), shear stress is proportional to $w^{-(n+1)}$, i.e., the smaller the crack opening, the larger is the shear stress. The numerical results also suggest that there is local crack closure near the tip of the fracturing fluid. Thus, the crack-closure phenomenon is not due to the singularity of the shear stress. A different structure of boundary layer shown in Fig. 10 is presented by using the full-stress model. The shear stress leads to a higher stress singularity in the outer solution. Different from the inner solution which is derived to interpret the failure of material, the outer solution is the result of the solid-fluid coupling. According to the stress distribution shown in Refs. [6,7], the maximum tensile stress in the outer solution is σ_{11} indicating potential presence of mode-I cracks perpendicular to the original crack surfaces.

Note that the crack closure in the fluid-tip region has not been reported in the laboratory and field experiments [16–19]. There are multiple reasons for the lack of observations of the crack-closure phenomenon, which likely include (1) structural instabilities in addition to the crack closure, (2) experimental conditions not suitable for the occurrence of the crack closure, and (3) the short duration of the crack closure. For the first case, the straight crack at the state of plain strain make it impossible to introduce structural instabilities, such as the deflection, branching, fingering and nonplanar propagation of the crack, while it is possible to have unstable crack propagation. For the second case, the characteristic length is physically limited by the grain sizes of rocks. According to Eqs. (34) and (40), the viscosity of the fracturing fluid is too small for the crack closure during the hydraulic fracturing of a well-prepared specimen with a crack. Also, the slow injection tends to prevent the occurrence of the crack closure since the dimensionless fracture

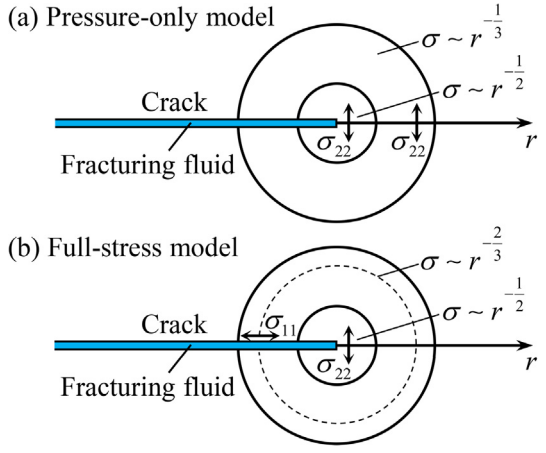

Fig. 10. Schematic of the boundary layers at the crack tip. The inner solution is in accord with the linear elastic fracture mechanics, while the outer solution is abnormal (the fracturing fluid is Newtonian); a) In a pressure-only model, maximum stress components in the two layers are σ_{22}, and b) in a full-stress model, the maximum stress component in the outer solution is σ_{11}.

toughness is large enough to counterbalance the effect of the shear stress. However, there are corners and variations in the fluid channel of which local resistance may be larger than the friction resistance [32]. An underestimated hydraulic resistance arises by simply using the fluid viscosity from laboratory experiments and the straight-crack assumption. For the third case, the duration of the crack closure may be so small that the associated pressure fluctuations measured are possibly treated as measurement errors. Further quantitative studies are required to consider the inertia effect and capture the details of crack closure including its duration.

Understanding the unstable crack growth caused by flow-induced shear stress likely provides valuable insight into the formation of hydraulic crack networks. There likely exist a variety of instabilities, such as deflection and non-planar propagation of a crack, which can create complex crack networks in rocks. In a hydrocarbon reservoir with depth larger than 3 km under the ground, where the crustal stress is larger than 50 MPa, the fluid-lag zone is negligible according to Eq. (47). Consequently, Eq. (40) can be used to predict unstable growth of cracks. In the perspective of numerical simulation, the crack-tip issues have long been the difficulties in developing computer programs [29], and the stress singularities and the potential instabilities discussed here are essential to develop novel numerical schemes. In the perspective of realistic hydraulic fracturing treatments of shale reservoirs, potential unstable crack growth is predicted. Even though producing a large number of instabilities is a method to form large-scale fracture networks, the model developed here is so simple that does not include the highly heterogeneous properties of shale rocks [33]. Further studies are needed to incorporate the heterogeneous properties of shale reservoirs and full-stress coupling at the solid-fluid interfaces.

5. Conclusions

The pressure-only model is extended to the full-stress model which takes into account of the combined effects of pressure and shear stress on the crack surfaces. The stress intensity factor is modified, and the strain energy release rate is derived, in which there is an additional contribution from singular shear stress. The full-stress model incorporates the physical effects of fracture, viscosity, shear stress, crustal stress and surface tension. Scaling analysis reveals the conditions when each effect is negligible. All the five physical effects play important roles in the crack propagation with the fluid-lag zone, and there are only three physical effects (fracture, viscosity and shear stress) determining the crack propagation without the fluid-lag zone. The effect of the shear stress gradually becomes less important during the fracturing, and the effect of fracture and surface tension depends on the flow behavior index of the fracturing fluid. For a shear-thinning fracturing fluid, the surface tension is negligible at large time; for a shear-thickening fracturing fluid, the surface tension becomes dominant at large time; and for a Newtonian fracturing fluid, the effect of the surface tension remains unchanged during the fracturing. The full-stress model degenerates to the pressure-only model for large times when the crack opening caused by the shear stress is negligible in comparison with that caused by the pressure. According to the full-stress analysis, the following conclusions can be drawn:

- Unstable crack growth can occur in the shear-stress-dominant regime. With the assumption of a straightly propagating fluid-driven crack, shear stress may lead to the crack closure near the fluid tip in the shear-stress-dominant regime. Due to two numerical constraints, shear stress leads to mesh-dependent results in the numerical calculations. For the cases without fluid-lag zone, an empirical necessary criterion for the crack closure is obtained. A fluid-driven crack with no fluid-lag zone closes much easier than that from the same model with a fluid-lag zone.
- The unstable crack growth is independent of the fluid-lag zone, indicating that the crack-closure phenomenon is not due to stress singularities. A new structure of boundary layer at the crack tip is predicted by the full-stress model. Shear stress leads to a higher stress singularity compared with hydrodynamic pressure in the outer solution. The outer solution predicts potential mode-I cracks in the direction perpendicular to the original crack surfaces.
- The lubrication theory is valid to describe the flow of fracturing fluid. The effect of two-dimensional flow is limited in the region in which the fluid-channel width is comparable with the length. Vertical velocity removes the pressure singularity. However, the singular pressure is integrable in the lubrication theory, and its effect on the crack propagation criterion is negligible for a crack with length much larger than its opening width. The discrepancy introduced by vertical velocity is negligible.
- In the toughness-dominant regime, the effect of shear stress are two folds. On the one hand, the shear stress leads to a narrower crack opening, a longer crack (mass conservation) and a lower wellbore pressure (crack propagates more easily for a longer crack); on the other hand, the shear stress decreases the stress intensity factor, resulting in a larger wellbore pressure, then a wider crack opening, and finally a longer crack (mass conservation). The former dominates the hydraulic fracturing for small times, and the latter takes effect for large time.
- There are multiple factors determining the size of the fluid-lag zone. The size of fluid-lag zone is estimated for small times, when the length of the fluid channel is much smaller than that of the fluid-lag zone. A small fluid-lag zone is obtained due to the shear stress and the crustal stress on the crack opening. The fluid-lag zone becomes increasingly negligible with time under the action of the crustal stress. The effect of the shear stress on the fluid-lag zone is limited to small time. The surface tension plays an important in microcracking, and a larger fluid-lag zone is obtained for a hydrophobic rock.

In the full-stress model, the rock is modeled as homogenous, isotropic, and linearly elastic, and incompressible fracturing fluid with power-law rheology is used. In hydraulic fracturing, multiple cracks can propagate at the same time, shale rocks are highly heterogeneous with a large number of joints and natural fractures, the shear-stress-induced volume dilatation can occur near crack tips, and the fracturing fluid flows together with an enormous amount of proppant [8,9]. The proposed model may not capture the details of unstable crack propagation including the crack paths, the evolving stress field and the duration. Further studies are needed to extend this model to simulate a more realistic hydraulic fracturing process.

This study provides a systematic analysis of the effect of the flow-induced shear stress on the unstable growth of a fluid-driven crack. The results shed insights into hydraulic fracturing in the hydrocarbon reservoirs of low permeability. It also suggests that there is a divergent solution in numerical simulation for an over-refined mesh being used near the crack tip.

Acknowledgments

This research is supported in part by the National Natural Science Foundation of China (NSFC, Grant Nos. 11872363, 51861145314, U1562105), and by the Chinese Academy of Sciences (CAS) through CAS Interdisciplinary Innovation Team Project, the CAS Key Research Program of Frontier Sciences (Grant No. QYZDJ-SSW-JSC019), the CAS Strategic Priority Research Program (Grant No. XDB22040401) and Opening Fund of State Key Laboratory of Nonlinear Mechanics (LNM).

Appendix A. Energy release rate and stress intensity factor in the toughness-dominant regime

In the toughness-dominant regime, the square-root singularity of stress field remains unchanged. The normal displacement component behind the crack tip and normal stress component in front of the crack tip for $\tau = \tau_0/\sqrt{1 - x_1^2/l^2}$ are [6]

$$u_2(x_1, 0^+) = \frac{2K_{\mathrm{Ip}}}{E'}\sqrt{\frac{2l}{\pi}}\sqrt{1 - \frac{x_1}{l}} + \frac{(1-2\nu)\sqrt{2}\tau_0 l}{(1-\nu)E'}\sqrt{1 - \frac{x_1}{l}} + O\left(1 - \frac{x_1}{l}\right), \quad x_1 \to l^- \tag{A.1}$$

$$\sigma_{22}(x_1, 0) = \frac{K_{\mathrm{Ip}}}{\sqrt{2\pi(x_1 - l)}} + O(1), \quad x_1 \to l^+ \tag{A.2}$$

where $K_{\mathrm{Ip}} = \lim_{x_1 \to l^+}\sqrt{2\pi(x_1 - l)}\sigma_{22}(x_1, 0)$. Substituting $u_2(x_1, 0^+)$ and $\sigma_{22}(x_1, 0)$ into the following strain energy release rate [14],

$$G = \lim_{\Delta l \to 0^+}\frac{2}{\Delta l}\int_0^{\Delta l}\frac{1}{2}\sigma_{22}(l + \zeta, 0^+)u_2(l + \zeta, 0^+)\mathrm{d}\zeta \tag{A.3}$$

and using the result of the definite integral, $\int_0^{\Delta l}\sqrt{(\Delta l - \zeta)/\zeta}\mathrm{d}\zeta = \pi\Delta l/2$, one obtains

$$G = K_{\mathrm{Ip}}\left[\frac{K_{\mathrm{Ip}}}{E'} + \frac{(1-2\nu)\sqrt{\pi l}\tau_0}{2(1-\nu)E'}\right] \tag{A.4}$$

The stress intensity factor can be also calculated as $K_{\mathrm{I}} = \lim_{x_1 \to l^+}\sqrt{2\pi(x_1 - l)}\sigma_{11}(x_1, 0^+)$, in which $\sigma_{11}(x_1, 0^+)$ is [14]

$$\sigma_{11}(x_1, 0^+) = \frac{2}{\pi}\frac{x_1}{\sqrt{x^2 - l^2}}\int_0^{x_1} p(\zeta)\frac{\sqrt{l^2 - \zeta^2}}{x_1^2 - \zeta^2}\mathrm{d}\zeta + \frac{4}{\pi}\int_0^l \frac{\tau(\zeta)\zeta\mathrm{d}\zeta}{x_1^2 - \zeta^2} \tag{A.5}$$

The first term in Eq. (A.5) is the same as that from $\sigma_{22}(x_1, 0^+)$, which gives the stress intensity factor as K_{Ip}. For $\tau = \tau_0/\sqrt{1 - x_1^2/l^2}$, the second term can be evaluated using

$$\int_0^1 \frac{\zeta\mathrm{d}\zeta}{\sqrt{1 - \zeta^2}(x^2 - \zeta^2)} = \frac{1}{\sqrt{x^2 - 1}}\arcsin\frac{1}{x} \tag{A.6}$$

Thus, the stress intensity factor from $\sigma_{11}(x_1, 0^+)$ is

$$K_{\mathrm{I}} = 2\sqrt{\frac{l}{\pi}}\int_0^l \frac{p(s)\mathrm{d}s}{\sqrt{l^2 - s^2}} + 2\sqrt{\pi l}\tau_0 \tag{A.7}$$

Appendix B. Numerical scheme for the model without fluid-lag zone

The Chebyshev polynomials are used to approximate the unknown functions as

$$\widetilde{\boldsymbol{w}} = \boldsymbol{a}\cdot\boldsymbol{T}, \ \widetilde{\boldsymbol{p}} = \boldsymbol{b}\cdot\boldsymbol{T}^{\mathrm{p}}, \ 2\widetilde{\tau} = \boldsymbol{c}\cdot\boldsymbol{T}^{\mathrm{t}}, \quad \text{and} \quad \partial_{\widetilde{x}_1}\widetilde{\boldsymbol{p}} = \boldsymbol{d}\cdot\boldsymbol{T}^{\mathrm{d}} \tag{B.1}$$

where $\boldsymbol{a}$, $\boldsymbol{b}$, $\boldsymbol{c}$ and $\boldsymbol{d}$ are constant vectors to be determined.

$$T_{ij} = \cos[i\arccos(1 - 2\widetilde{x}_{1j})], \ T_{ij}^{\mathrm{p}} = (1 - \widetilde{x}_{1j}^2)^{e_{\mathrm{p}}}T_{ij}, \ T_{ij}^{\mathrm{t}} = (1 - \widetilde{x}_{1j}^2)^{e_{\mathrm{t}}}T_{ij} \ \text{ and } \ T_{ij}^{\mathrm{d}} = (1 - \widetilde{x}_{1j}^2)^{e_{\mathrm{p}}-1}T_{ij}, \quad i, j = 0\sim N - 1 \tag{B.2}$$

where N is the number of polynomials used, a larger N gives a higher accuracy of the numerical results; e_{p} and e_{t} are two auxiliary constants representing the exponents of the pressure and the shear stress at the crack tip, respectively. The terms of $(1 - \widetilde{x}_1^2)^{e_{\mathrm{p}}}$ and $(1 - \widetilde{x}_1^2)^{e_{\mathrm{t}}}$ are used to represent the singularities at $\widetilde{x}_1 = 1$ and to improve the numerical calculation. Thus, the integro-differential equations reduce to algebraic equations which can be numerically solved. Here, $1 - \widetilde{x}_{1j}^2$ is used due to the symmetric characteristic of the crack about the $O\widetilde{x}_2$ axis; all of the variables are even functions of $\widetilde{x}_1$. In the interval (0, 1), $1 - 2\widetilde{x}_1$ is used to satisfy the domain requirement of the Chebyshev polynomials. The constant vector of $\boldsymbol{a}$ for an arbitrary known function of $f(x)$ in (0, 1) is calculated as

$$\boldsymbol{a} = \boldsymbol{f}\cdot\boldsymbol{A} \tag{B.3}$$

in which $A_{ij} = (2 - \delta_{0i})\cos[i\pi(j + 1/2)/N]/N$, δ_{0i} is the Kronecker delta, $f_i = f(x_i)$, and $x_i = 1/2 - \cos[(2i + 1)\pi/2N]/2$ (the i - th point in Gaussian quadrature). From Eq. (B.3), the function of $f(x)$ can be approximated as

$$f(x) = \sum_{i=0}^{N-1} a_i T_i(1 - 2x) \tag{B.4}$$

The numerical analysis was focused first on the calculation of the constant vectors of $\boldsymbol{a}$, $\boldsymbol{b}$, $\boldsymbol{c}$ and $\boldsymbol{d}$. Using the Chebyshev approximation of Eq. (B.1), one obtains the discretized Eqs. (24)–(27) as

$$\widetilde{l} = \frac{\widetilde{t}}{\boldsymbol{f}_1 \boldsymbol{a}} \tag{B.5}$$

$$\partial_{\widetilde{x}_1}\widetilde{\boldsymbol{p}} = -\frac{\widetilde{l}}{\widetilde{\boldsymbol{w}}^{2n+1}}\left[\left(\frac{\widetilde{l}}{\Delta\widetilde{t}} + \frac{\widetilde{l} - \widetilde{l}_0}{\Delta\widetilde{t}}\right)\boldsymbol{a}\cdot\boldsymbol{f}_5 - \frac{\widetilde{l}}{\Delta\widetilde{t}}\boldsymbol{a}_0\cdot\boldsymbol{f}_5 + \frac{\widetilde{l} - \widetilde{l}_0}{\Delta\widetilde{t}}\widetilde{\boldsymbol{x}}.*\widetilde{\boldsymbol{w}}\right]^n \tag{B.6}$$

$$\widetilde{\boldsymbol{w}} = \widetilde{l}\,\widetilde{\boldsymbol{a}}\cdot\widetilde{\boldsymbol{f}}_3 + \widetilde{Q}\widetilde{\boldsymbol{c}}\cdot\widetilde{\boldsymbol{f}}_4 \tag{B.7}$$

$$\widetilde{\boldsymbol{p}} = \frac{2}{\pi}\left(\frac{\widetilde{K}_{\mathrm{IC}}}{\sqrt{\widetilde{l}}} - \boldsymbol{d}\cdot\boldsymbol{f}_2\right) + \boldsymbol{d}\cdot\boldsymbol{f}_6 \tag{B.8}$$

and the shear stress is calculated with $\widetilde{\tau} = (\widetilde{\boldsymbol{w}}/2).*\partial_{\widetilde{x}_1}\widetilde{\boldsymbol{p}}$, where $\boldsymbol{a}.*\boldsymbol{b}$ represents the vector $\{a_i b_i\}$; the subscript "0" represents the initial condition in a single time step; and $\boldsymbol{f}_1$ to $\boldsymbol{f}_6$ are defined by

$$f_{1j} = \int_0^1 T_j(1 - 2\zeta_1)\mathrm{d}\zeta \tag{B.9}$$

$$f_{2j} = \int_0^1 \arccos(\zeta) T_j(1 - 2\zeta)(1 - \zeta^2)^{e_p - 1}\mathrm{d}\zeta \tag{B.10}$$

$$f_{3ij} = \frac{2}{\pi}\int_0^1 T_j(1 - 2\zeta)(1 - \zeta^2)^{e_p} ln\frac{\sqrt{1 - \widetilde{x}_{1i}^2} + \sqrt{1 - \zeta^2}}{\sqrt{|x_{1i}^2 - \zeta^2|}}\mathrm{d}\zeta \tag{B.11}$$

$$f_{4ij} = \int_{\widetilde{x}_{1i}}^1 T_j(1 - 2\zeta)(1 - \zeta^2)^{e_t}\mathrm{d}\zeta \tag{B.12}$$

$$f_{5ij} = \int_{\widetilde{x}_{1i}}^1 T_j(1 - 2\zeta)\mathrm{d}\zeta \tag{B.13}$$

$$f_{6ij} = \int_{\widetilde{x}_{1i}}^1 T_j(1 - 2\zeta)(1 - \zeta^2)^{e_p - 1}\mathrm{d}\zeta \tag{B.14}$$

An iterative method is used to solve the system of linear algebraic equations. The initial crack opening of $\widetilde{\boldsymbol{w}}^0$ is assumed as elliptical and recalculated with Eq. (26). In the numerical calculation, the results from the last step is used as the initial values in the next calculation. The iterative process includes: (i) the calculation of $\boldsymbol{f}_1$ to $\boldsymbol{f}_6$; (ii) iteration with the calculation of the pressure gradient, the shear stress, the pressure, and the constant vectors $\boldsymbol{a}$, $\boldsymbol{b}$, $\boldsymbol{c}$; (iii) the calculation of a new crack opening $\boldsymbol{w}'$ from Eq. (B.7); and (iv) the calculation of the relative difference, ε_w, of the crack openings between adjacent iterations; if ε_w is less than a pre-determined value, the iteration stops; if not, the crack opening is re-calculated as $(1 - \Delta_w)\widetilde{\boldsymbol{w}} + \Delta_w\widetilde{\boldsymbol{w}}'$, with Δ_w being the relaxation factor. A new time step starts after finishing the iteration.

References

[1] Khristianovic SA, Zheltov YP. Formation of vertical fractures by means of highly viscous fluids. Proc 4th World Petroleum Congress. 1955. p. 579–86.
[2] Geertsma J, de Klerk F. A rapid method of predicting width and extent of hydraulically induced fractures. J Petrol Technol 1969;21(12):1571–81.
[3] Spence DA, Sharp P. Self-similar solutions for elastohydrodynamic cavity flow. Proc R Soc Lond A-Math Phys Sci 1819;1985(400):289–313.
[4] Tsai VC, Rice JR. A model for turbulent hydraulic fracture and application to crack propagation at glacier beds. J Geophy Res-Earth 2010;115(F3):F03007.
[5] Yang FQ, Zhao YP. The effect of a capillary bridge on the crack opening of a penny crack. Soft Matter 2016;12(5):1586–92.
[6] Shen W, Zhao YP. Quasi-static crack growth under symmetrical loads in hydraulic fracturing. J Appl Mech-T ASME 2017;84(8):081009.
[7] Shen W, Zhao YP. Combined effect of pressure and shear stress on penny-shaped fluid-driven cracks. J Appl Mech-T ASME 2018;85(3):031003.
[8] Yew CH, Weng X. Mechanics of hydraulic fracturing. Oxford, UK: Gulf Professional Publishing; 2014.
[9] Valk P, Economides MJ. Hydraulic fracture mechanics. New York: Wiley; 1995.
[10] Garagash D, Detournay E. The tip region of a fluid-driven fracture in an elastic medium. J Appl Mech-T ASME 2000;67(1):183–92.
[11] Detournay E. Mechanics of hydraulic fractures. Annu Rev Fluid Mech 2016;48(1):311–39.
[12] Huang X, Zhao YP. Characterization of pore structure, gas adsorption, and spontaneous imbibition in shale gas reservoirs. J Petrol Sci Eng 2017;159:197–204.
[13] Lawn BR. Fracture of brittle solids. Cambridge University Press; 1993.
[14] Zhao YP. Modern continuum mechanics. Beijing: Science Press; 2016.
[15] Bui H, Parnes R. A reexamination of the pressure at the tip of a fluid-filled crack. Int J Eng Sci 1982;20(11):1215–20.
[16] Bohloli B, De Pater C. Experimental study on hydraulic fracturing of soft rocks: Influence of fluid rheology and confining stress. J Petrol Sci Eng 2006;53(1):1–12.
[17] Lecampion B, Desroches J, Jeffrey RG, Bunger AP. Experiments versus theory for the initiation and propagation of radial hydraulic fractures in low-permeability

materials. J Geophysl Res-Sol Ea 2017;122(2):1239–63.
[18] Lai CY, Zheng Z, Dressaire E, Ramon GZ, Huppert HE, Stone HA. Elastic relaxation of fluid-driven cracks and the resulting backflow. Phys Rev Lett 2016;117(26):268001.
[19] Cleary MP, Wright CA, Wright TB. Experimental and modeling evidence for major changes in hydraulic fracturing design and field procedures. SPE Gas Technology Symposium. Society of Petroleum Engineers; 1991.
[20] Batchelor GK. An introduction to fluid dynamics. Cambridge University Press; 2000.
[21] Zhao YP. Physical mechanics of surfaces and interfaces. Beijing: Science Press; 2012.
[22] Warpinski NR, Moschovidis Z, Parker C. Abou-Sayed I. Comparison study of hydraulic fracturing models—test case: GRI staged field experiment No. 3. SPE Prod Facil 1994;9(01):7–16.
[23] Garagash D. Transient solution for a plane-strain fracture driven by a shear-thinning, power-law fluid. Int J Numerl Anall Met 2006;30(14):1439–75.
[24] Van Dyke M. Slow variations in continuum-mechanics. Adv Appl Mech 1987;25:1–45.
[25] Sedov LI. Similarity and dimensional methods in mechanics. Boca Raton, Florida: CRC Press; 1993.
[26] Barenblatt GI. Scaling, self-similarity, and intermediate asymptotics: dimensional analysis and intermediate asymptotics. Cambridge: Cambridge University Press; 1996.
[27] Zhao YP. Nano and mesoscopic mechanics. Beijing: Science Press; 2014.
[28] Mishuris G, Wrobel M, Linkov A. On modeling hydraulic fracture in proper variables: Stiffness, accuracy, sensitivity. Int J Eng Sci 2012;61:10–23.
[29] Lecamplon B, Detournay E. An implicit algorithm for the propagation of a hydraulic fracture with a fluid lag. Comput Method Appl M 2007;196(49–52):4863–80.
[30] Pepper DW, Kassab AJ, Divo EA. An introduction to finite element, boundary element, and meshless methods with applications to heat transfer and fluid flow. New York: American Society of Mechanical Engineers; 2014.
[31] Linkov AM. On decaying influence of initial conditions in the problem of hydraulic fracturing. Dokl Phys 2016;61(7):351–3.
[32] Idelchik IE, Fried E. Handbook of hydraulic resistance. Washington: Hemisphere Publishing Corporation; 1986.
[33] Norris JQ, Turcotte DL, Moores EM, Brodsky EE, Rundle JB. Fracking in tight shales: What is it, what does it accomplish, and what are its consequences? Annu Rev Earth Pl Sc 2016;44:321–51.